Proton exchange membrane water electrolysis using sulfo-phenylated polyphenylene as membrane and ionomer

by

Xin Wang

B.Sc. (Chemistry), St. Francis Xavier University, 2018

B.E. (Chemical Engineering and Technology), Changzhou University, 2018

Thesis Submitted in Partial Fulfillment of the

Requirements for the Degree of

Master of Science

in the

Department of Chemistry

Faculty of Science

SIMON FRASER UNIVERSITY

Fall 2021

Declaration of Committee

Name:	**Xin Wang**
Degree:	**Master of Science (Chemistry)**
Title:	**Proton exchange membrane water electrolysis using sulfo-phenylated polyphenylene as membrane and ionomer**
Examining Committee:	**Chair:** Paul Li Professor, Chemistry
	Steven Holdcroft Supervisor Professor, Chemistry
	Caterina Ramogida Committee Member Assistant Professor, Chemistry
	Zuoguang Ye Committee Member Professor, Chemistry
	Loren Kaake Examiner Associate Professor, Chemistry

Abstract

Perfluorosulfonic acid (PFSA) based ionomers such as Nafion® are the technological standard for use in state-of-the-art proton exchange membrane water electrolysis (PEMWE) because of its high proton conductivity and excellent mechanical, chemical, and thermal stability. However, increasing environmental concerns with fluorinated polymers and safety issues associated with high gas crossover in PEMWE systems call for alternatives to PFSAs. A wholly hydrocarbon-based PEM sulfonated phenylated polyphenylene biphenyl (sPPB-H^+), which has already been employed in proton exchange membrane fuel cell (PEMFC) systems is considered a candidate material for PEMWE as it exhibits high proton conductivity and mechanical robustness. The validation of sPPB-H^+ as a membrane and ionomer applied in the catalyst layer in membrane electrode assembly (MEA) structures is evaluated in an electrolyzer cell. When using Nafion D520™ in the catalyst layer, a sPPB-H^+ membrane yields better energy efficiency than a reference Nafion™112 membrane. The enhanced energy efficiency is attributed to significantly lower ohmic resistance. The use of sPPB-H^+ as ionomer is also investigated, where maximum efficiency is achieved by determining the optimal ionomer content.

The stability of MEAs in electrolyzers is studied by monitoring the voltage change at a constant current density. Degradation mechanisms of MEAs are elucidated using polarization curves, EIS and hydrogen gas crossover measurements. Initially, sPPB-H^+ membranes yield substantial lower gas crossover compared to the Nafion 112 membrane. As PPB-H^+ is prone to radical attack, the membrane develops pinholes allowing increasing gas crossover. The rapid performance decay (i.e., much higher voltage evolution rate) of wholly hydrocarbon sPPB-H^+ based MEAs is initially caused by severe catalyst loss and increasing gas crossover due to thinning of the catalyst layers.

The results presented here demonstrate sPPB-H^+ as a promising material for application in water electrolysis and suggest future research should focus on mitigating chemical degradation and reducing dimensional swelling of the membrane in order to enhance its operational stability.

Keywords: PEM water electrolysis; hydrocarbons; sulfonated poly(phenylene); ionomer; membrane electrode assembly; gas crossover

Acknowledgements

Foremost, I would like to express my great appreciation to my supervisor Dr. Steven Holdcroft, for giving me the opportunity to work in his group since 2018. I am very grateful for his guidance, support, extraordinary patience and encouragement throughout my study in SFU for the last three years.

I highly appreciate my supervisory committee membranes, Dr. Caterina Ramogida and Dr. Zuoguang Ye for their supervision and encouragement.

I also wish to thank Dr. Xin Zhang for his guidance in SEM technique and generously lend me conductivity meter.

To the past and present group members, thank you for the happy and good time we spent together in the lab, especially for Dr. Thomas Skalski, Dr. Mike Adamski, Dr. Simon Cassegrain, Dr. Qiliang Wei, Emmanuel Balogun, XinZhi (Sydney) Cao. I would like to thank Amelia Hohenadel for guiding me when I first entered the lab, as well as Binyu Chen for his valuable discussion and contribution to this research. I am particularly grateful to Dr. Peter Mardle for constructive guidance and suggestions in finishing this thesis.

And finally, to my mother, my family and my friends for their endless love.

Table of Contents

List of Tables

List of Figures

List of Symbols and Abbreviations

AEM	Anion exchange membrane
AWEWE	Alkaline water electrolysis water electrolysis
EIS	Electrochemical impedance spectroscopy
EW	Equivalent weight
HER	Hydrogen evolution reaction
IEC	Ion exchange capacity
IPA	Isopropyl alcohol
MEA	Membrane electrode assembly
OER	Oxygen evolution reaction
PBI	Polybenzimidazoles
PEEK	Poly (ether ether ketones)
PEM	Proton exchange membrane
PEMWE	Proton exchange membrane water electrolysis
PES	Poly (ether sulfones) (PES)
PPQ	Polyphenyl quinoxaline
PTFE	Polytetrafluoroethylene
PTLs	Porous transport layers
RH	Relative humidity
sPEEK	Sulfonated poly (ether ether ketones)
sPPB-H^+	Sulfonated phenylated polyphenylene biphenyl
sPPP	Sulfonated, phenylated poly(phenylene)s
sPPS	Sulfonated poly (phenylene sulfone)
sPSf	Sulfonated poly(polysulfone)
TCD	Thermal conductivity detector
TPA	Tungstophosphoric acid

A	Area, m^2
C	Capacitor
C_i	Molarity of titrant, mol L^{-1}
C_{NaOH}	Concentration of charge carrier, mol cm^{-3}
E	Potential, V
F	Faraday constant, 96485 C mol^{-1}
G	Gibbs free energy
I	Current, A
L	Inductor
R	Resistor
$R_Ω$	Ohmic resistance, Ω cm^2
R_{CT}	Charge transfer resistance, Ω cm^2
R_{el}	Electrolyte resistance, Ω
U_i	Mobility of carrier, cm^2 V^{-1} s^{-1}
V	Voltage, V
V_{NaOH}	Volume of titrant, L
Z	Electrical Impedance, Ω cm^2
Z_i	Charge number of the carrier
λ	Water content, mol H_2O /mol SO_3H
σ_i	Proton conductivity, S cm^{-1} or $Ω^{-1}$ cm^{-1}
ϕ	Phase shift
ω	Weight, g
$ω_{dry}$	Weight of the dry polymer, g

Chapter 1.

Introduction

1.1. Water electrolysis

1.1.1. Hydrogen produced by water electrolysis: a brief background

Fossil fuels are the dominant energy resource and have driven global technological, social, and economic development since the Industrial Revolution. Between 2013-2020, fossil fuels accounted for > 80% of global energy demand. The massive consumption of petroleum, coal and natural gas, the limited nature of these fossil fuels and related environmental issues such as greenhouse gas emissions are calling for a shift to clean renewable energy sources. However, the intermittent nature of renewable energies like wind, solar, and hydroelectric, prevents them from providing sustainable energy in a continuous manner. Therefore, systems which permit renewable energy to be stored when it is in surplus, and to be released upon demand, are widely considered to be solutions to this dilemma, improving the reliability, quality and economics of renewable energy.[1,2]

Hydrogen is considered one of the best solutions for surplus energy storage from intermittent power sources such as wind and solar electricity. Hydrogen has high energy content (118 MJ kg^{-1}, 298K) which is two or three times higher than most other common fuels (e.g., gasoline 44 MJ kg^{-1}). Hydrogen can also be stored in gaseous or liquid form for long distance transport and used directly as a fuel for heating, transportation, in the chemical industry or oxidized to water in a fuel cell, converting the stored chemical energy into electricity.[1,2,3] The technology that enables hydrogen to bridge renewable electrical generation and end-use application is water electrolysis.

Water electrolysis can generate high-purity hydrogen in large quantities using electricity. There are two commercially available low-temperature water electrolysis technologies —alkaline water electrolysis (AWE), and proton exchange membrane water electrolysis (PEMWE). Anion exchange membrane water electrolysis (AEMWE) which

could combine advantages of both alkaline water electrolysis and PEMWE, is still a developing technology.[1,2,3,4]

Alkaline water electrolysis has existed since the late 1800s and developed in 1920s and 1930s to produce hydrogen at scales of 10,000 $Nm^3\ h^{-1}$ (the prouction rate was measured at standard condition of 0 ℃ and 1 atm). Today, sizeable alkaline water electrolysis plants exist, for example, at Aswan Dam in Egypt, Nangal in India, Glomfjord in Norway and Trial in Canada.[5,6] Commercial alkaline water electrolyzer stacks typically contain 2 to 300 or more cells connected and operate at current densities around 200 to 500 mA cm^{-2} at 80 ℃ and 1.8 V.[7,8] Alkaline electrolyzers are operated by circulating concentrated KOH at each electrode, separated by a porous diaphragm separator, typically made of non-electron conductive Zirfon™. A big gap between two electrodes results in high ohmic resistance, limiting operating current density and bulky stack designs to meet hydrogen production demand. Additionally, as the diaphragm cannot wholly prevent gas crossover, alkaline KOH electrolyzers are usually operated at atmospheric or low pressure (< 30 bar), resulting in further energy costs associated with downstream H_2 compression.[5,9] Proton exchange membrane (PEM) electrolyzers replace the separator with a thin solid polymer electrolyte PEM, solving some of these issues.

The first PEM electrolyzer system was developed by General Electric in 1955 and the technology was sold to Hamilton Sundstrand in 1985 for space and submarine applications.[5] Current manufacturers of PEM stacks for example include Giner Inc (US), UTC Aerospace Systems (US), NEL (Norway), Hydrogenics (CA), Siemens (DE), Norsk Hydro ASA (NO), and the Kurchatov Institute (RU).[8,10] The hydrogen production capacity of a PEM water electrolyzer is up to several hundreds $Nm^3\ h^{-1}$. Due to the introduction of the PEM, proton exchange electrolyzers allow high current density operation (more than twice that of alkaline water electrolysis[11]), resulting from a much reduced distance between the anode and cathode electrodes which also allows for compact stack design. With low gas permeability, high operation pressure (balanced or differential) is accessible (up to 350 bar) decreasing the relative volume of gas in water, affording higher kinetic and mass transport through PTLs, and also allowing the direct storage and delivery of hydrogen in pressurized vessels.[9,12,13] In addition to the reduced ohmic resistance and the high operational pressure allowed by the “zero gap” between electrodes, PEMWE system has many other advantages; high efficiency, dynamic

behavior and rapid response.[4,5,14] These make PEMWE ideal for either grid stabilization or directly coupling with renewable energy sources. To increase participation of PEMWE systems in hydrogen markets and widespread commercialization, further investigations and improvements are required, especially regarding membrane stability, stack robustness, ease of operation and cost reduction.[1,2,15]

1.1.2. Principles of PEMWE

The basic design of a research-scale single cell PEM water electrolyzer with its main components is illustrated below (**Figure 1-1**). The two half-cells are separated by the solid, acidic PEM. Catalyst layers are commonly deposited directly onto either side of membrane and become cathode and anode of the water electrolyzer. Pt is an excellent catalyst for hydrogen evolution reaction (HER) due to high activity and stability. Ir-based catalysts are the state-of-the-art catalyst materials for oxygen evolution reaction (OER) at anode.[16] The combination of PEM and two electrodes creates the key component of a PEM electrolyzer, the membrane electrode assembly (MEA).

The MEA is where the water splitting occurs. It is sandwiched between porous transport layers (PTLs). The most widely used PTL for PEMWE are Ti-based materials, such as sintered Ti or Ti felts due to their stability in acidic environments.[17] The PTLs allow the flow of electric current, but more importantly the porosity of PTLs helps to distribute reactant water evenly to the catalysts and remove generated gas away from the reaction sites to the flow field channels, which are machined into the end plates that enclose and support the MEA. The flow field plates provide electrical contact to the external power supply and the flow paths provide even distribution of liquid water and the gases produced. Gaskets are also commonly used inside the cell to prevent water and gas leakage.

During operation, an external power source is applied to the cell to provide the energy for the non-spontaneous water splitting reaction, as well as excess potential energy to overcome electrical, ionic and electrochemical resistances. Water is oxidized at the anode according to Equation 1.1 to produce oxygen. Protons transport through the PEM from anode to cathode, where they are reduced by the electrons from the external circuit into hydrogen gas, as shown in Equation 1.2.

$H_2O(l) \rightleftarrows \frac{1}{2}O_2(g) + 2e^- + 2H^+(aq)$ anode $E^\circ(\text{OER})$ = 1.23 V vs. RHE **1.1**

$2H^+(aq) + 2e^- \rightleftarrows H_2(g)$ cathode E° (HER)= 0.00 V vs. RHE **1.2**

$H_2O(l) \rightleftarrows \frac{1}{2}O_2(g) + H_2(g)$ overall E°_{cell}= -1.23 V **1.3**

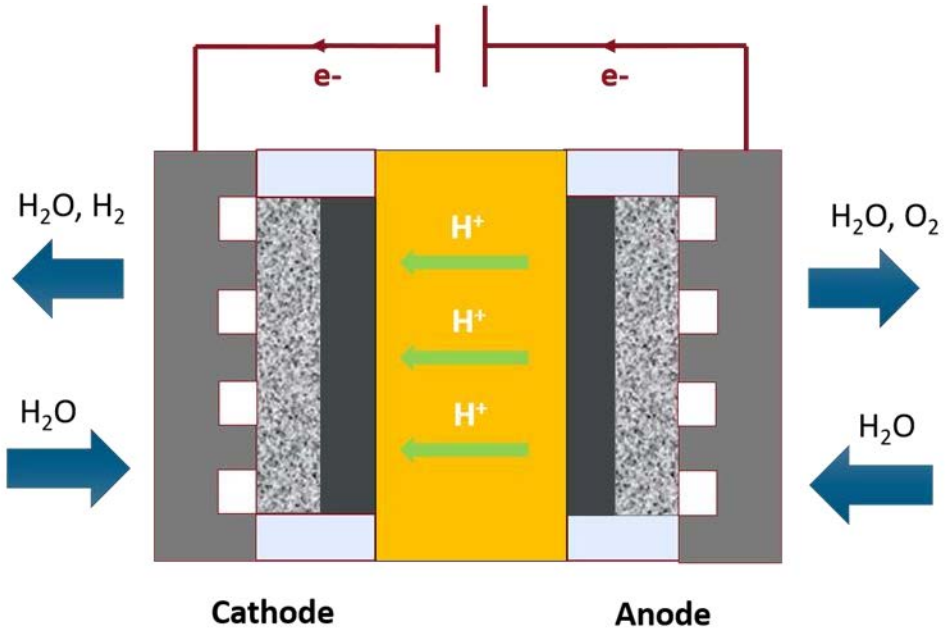

Figure 1-1 Schematic of a single proton exchange membrane (PEM) water electrolyzer cell with MEA assembled; from center outwards, the components are the PEM, catalyst layers, porous transport layers, flow fields embedded into current collectors. The cell is sealed by gaskets on top and below the catalyst layers and porous transport layers.

The combination of cathode and anode half-reactions gives an overall water electrolysis reaction (Equation 1.3). From this equation, the splitting of one mole of product water is a two-electron process with a resulting E^o_{cell} of -1.23 V, the theoretical minimum cell voltage required for water electrolysis at this temperature. This voltage is related to the thermodynamic Gibbs free energy ΔG (in kJ mol^{-1}) for water splitting by the following Equation 1.4:

$\Delta G = -nFE^\circ_{cell} = nFE_{rev}$ **1.4**

where n is the number of electrons transferred per reaction (n=2) and F is the Faraday's constant (96,485 C mol^{-1}). The change in Gibbs free energy ΔG for splitting liquid water at 25 °C is +237 kJ mol^{-1}.

The resulting E^{o}_{cell} calculated 1.23 V, is the theoretical minimum cell voltage required for water electrolysis at this temperature, namely, the reversible voltage for water electrolysis. Accounting for the generation of entropy ΔS (J mol^{-1} K^{-1}), it is more suitable to replace Gibbs free energy ΔG with enthalpy ΔH (kJ mol^{-1}) (Equation 1.5):

$$\Delta H = \Delta G + T\Delta S = nFV_{TN} \quad \textbf{1.5}$$

where T is temperature (in K) and V_{TN} is the thermo-neutral voltage. As the change of enthalpy ΔH is 286 kJ/mol, the calculated V_{TN} is 1.48 V. The energetic efficiency of electrolysis is calculated from the yield of converting overall energy input into chemical energy (Equation 1.6).[18,19]

$$\eta_E = \frac{V_{TN}}{V_{cell}} \quad \textbf{1.6}$$

1.2. The role of ionomers in PEMWE

An ionomer is a term given to an ion conductive polymer (polymer electrolyte) that consists of a low fraction of ions attached to the polymer chain. In the field of fuel cell science this term has been adopted to include all polymer electrolytes but in particular the polymer electrolyte incorporated into catalyst layers.[20] PEMs are cast from polymer electrolytes that possess negatively charged (anionic) groups to facilitate proton transportation. Sulfonic, phosphonic, and carboxylic groups are the strongest acidic functional groups and they have relatively small pK_a. Many other functional groups such as R-SH and R-OH behave as weaker acids. Among these three acidic functional groups, carboxylic acid group has the largest pKa, which means the number of dissociated mobile protons from the carboxylic group is low. Phosphonic acid groups can easily forms anhydrides at low relative humidity (RH), and as a result, the conductivity of protons may decrease dramatically unless operating at high temperature.[21] Therefore,

sulfonic acids are the favored choice of pendent functional group for proton exchange membranes at near ambient temperature conditions.[22]

The dissimilar nature of the electrically neutral backbone and bonded ionic acid groups result in the natural phase separation of the ionomer in water. The phase separation gives PEM the proton transport capability.[23] There are three conceivable mechanisms of proton transportation in PEM: the vehicular, the Grotthuss and the surface mechanism as shown in **Figure 1-2**. The vehicle-type mechanism describes proton migration through water channels along with the surrounding water as a "vehicle", e.g., H_3O^+, $H_5O_2^+$ and $H_9O_4^+$. The Grotthuss-type (hopping) mechanism elucidates the proton transferring from one entity to another through the breaking and formation of hydrogen bonding. When in low relative humidity (RH), protons can only move along the side chains under the electrostatic effects provided by the sulfonic acid groups, the so-called surface mechanism.[24,25,26]

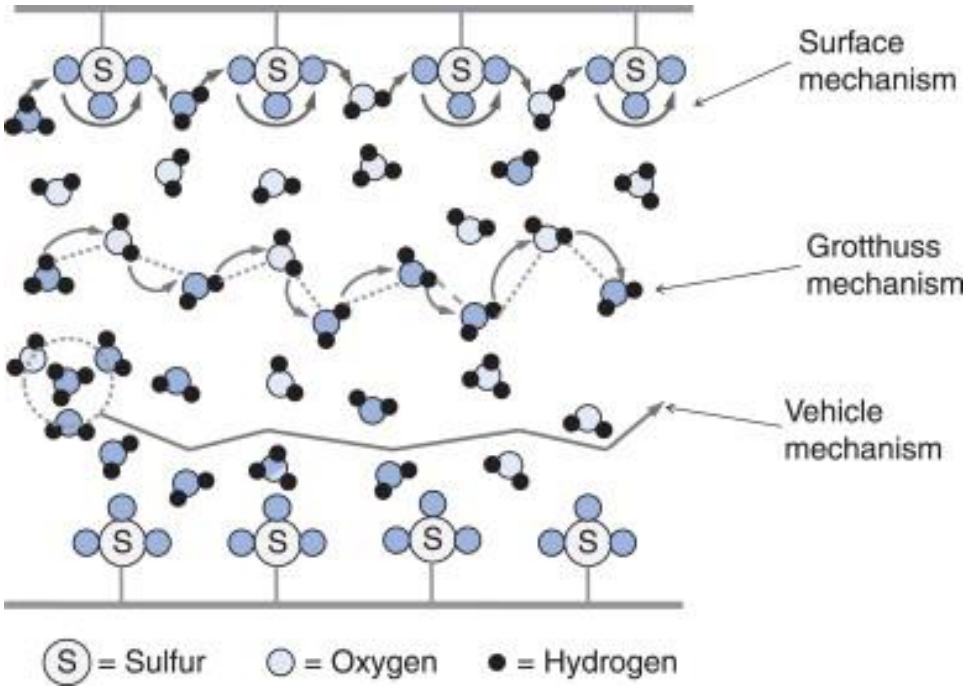

Figure 1-2 Scheme of proton tranfer mechanism (vehicle, Grotthuss and surface mechanism) in hydrated proton exchange polymer. Reprinted with permission from reference 25. Copyright 2006 Wiley.

1.2.1. Properties of PEMs

The concentration of acid groups available to conduct protons is characterized by the ion exchange capacity (IEC), millimole equivalent per gram of dry membrane or by the equivalent weight (EW), grams dry polymer per mole of ion exchange sites, where IEC=1000/EW.[27] IEC is generally determined by a conventional acid–base titration technique: the membrane is soaked in a concentrated NaCl (pH=7) solution to exchange proton counter-ions ($-SO3^-$ H^+) to sodium ($-SO3^-$ Na^+). The acidic solution is then titrated to pH 7 using the NaOH titrant. IEC (meq g^{-1}) can be calculated from the amount titrant used using the following equation:[28]

$$IEC = \frac{C_{NaOH}V_{NaOH}}{\omega_{dry}} \quad \textbf{1.5}$$

where C_{NaOH} is the molarity of titrant, V_{NaOH} is the volume of titrant and ω_{dry} is the weight of the dry polymer.

Ionic conductivity is used to quantify how well a material transports the counter-ions and describes how many charge carriers are and how easily they can move with a potential gradient. It is generally determined using the following equation:

$$\sigma_i = (|Z_i F|)c_i u_i \quad \textbf{1.6}$$

where Z_i is the charge number of the carrier, F is the faraday constant (96485 C mol^{-1}), C_i is the concentration of carrier and u_i is the mobility (cm^2 V^{-1} s^{-1}) of charge carrier. Therefore, the proton conductivity [σ, (S cm^{-1})] in PEMs is intrinsically governed by IEC as well as mobility of the protons, determined by the free volume in the PEM.[29]

Proton conductivity is usually measured with a two-electrode electrochemical impedance spectroscopy (EIS) technique and can be measured in two directions: *in-plane* and *through-plane*. Holdcroft and co-workers investigated the proton conductivity of membranes both *in-plane* (length/width dependent) and *through-plane* (thickness dependent) and concluded that *through-plane* conductivity is more appropriate for electrochemical devices (i.e., fuel cells and water electrolyzers). There are two main reasons: First, the morphological anisotropy of the membrane materials. Second, proton transportation are in the direction perpendicular to the membrane surface in the real cell.[30] However measuring *through-plane* conductivity is more difficult compared to

measuring *in-plane* conductivity due to the larger contact resistance contribution from the membrane and electrodes.[30] *In-plane* conductivity therefore are widely carried out for characterization of membrane proton conducting performance and the proton conductivities reported in most literature are *in-plane* conductivity.[28,31]

Proton conductivity should be discussed with water uptake as water promotes the dissociation. There are two forms of water uptake: weight pecent of water (ω) and water contant (λ). Weight percent of water (ω) is calculated based on the weight of the wet sample and dry sample:

$$\omega = \frac{\omega_{wet} - \omega_{dry}}{\omega_{dry}} \times 100\ \% \quad \textbf{1.7}$$

Water contant (λ) is the number of water molecules per sulfonic acid groupbet of the PEM:

$$\lambda = \frac{\omega \times EW}{M_{\mathrm{H2O}}} \quad \textbf{1.8}$$

where EW is the equivalent weight and M_{H_2O} is the molar weight of water.[32]

When fully hydrated in water, a membrane swells in both directions: *in-plane* (length/width) and *through-plane* (thickness). Swelling is due to a complex interplay between the affinity of the ionomer and water and the resistance of the membrane's structure and crystallinity to volumetric expansion.[32] Appropriate swelling is necessary for ionic mobility but the excess swelling needs to be avoided and may even cause dissociation of the membrane in the application.[28,31]

Low gas permeability is also an important property for membranes. As H_2 and O_2 are soluble in water, they can transport through a well-hydrated membrane to the opposite compartment of electrolyzer cell and cause contamination of product gas.[1,33,34]

The gas crossover is mainly caused by solution-diffusion mechanism as one of the crossover routes sketched in **Figure 1-3**. The dissolved gas can diffuse through water filled channels in the electrolyte membrane layer. The driving force is the Brownian motion and concentration gradient.[34] In addition to diffusion, to a lesser extent, there could be some convective transport caused by pressure and thermal differences

between anode and cathode. Finally, electroosmotic water drag can occur, where dissolved hydrogen and oxygen accompany proton migration from anode to cathode.[34]

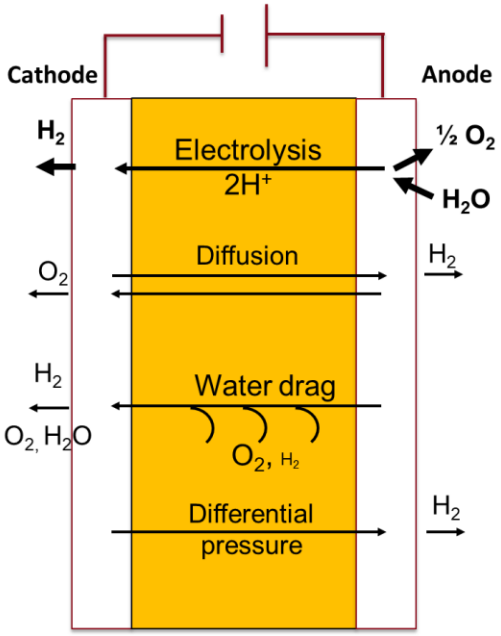

Figure 1-3 Gas crossover transport mechanism through 1) diffusion of hydrogen to anode and oxygen to cathode and 2) convective transport caused by electro-osmotically water drag and pressure difference between anode and cathode.

The hydrogen crossover is considered more critical than oxygen crossover. The reason for that is firstly, the permeability of oxygen is lower than that of hydrogen and the production rate of oxygen is only half that of hydrogen. Secondly, at the cathode, oxygen is reduced electrochemically by Pt to water resulting in a net zero product formation for the associated current. At the anode however, H_2 does not readily oxidize on the Ir based catalysts and so causes contamination of the product gas. With a lower explosion limit of 3.9 vol% in O_2, this is a safety issue.[1,34,35] The crossover and resulting safety concerns limit the obtainable pressurization of cathode and call for appropriate mitigation measures.

Overall, due to the complexity of PEMWE cells, harsh and dynamic operation condition, the PEM must possess the following desirable properties: high proton conductivity, low gas permeability for safe operation, and high mechanical, chemical, and thermal stability for practical applications.

1.2.2. Ionomer in the catalyst layer

Ionomer can be dispersed with catalysts/support to make an ink to be deposited on the surface of a membrane or PTL to form the electrodes/catalyst layers.[9,32] Typically, in a catalyst layer in **Figure 1-4**, ionomer is used as a binder to promote the exchange of protons from the bulk of membrane to the inside of catalyst layer.[38,39] It additionally impacts pore formation during deposition. Pores in the catalyst layer are vital for transporting reactant water to and from the reaction site and allowing product gas to expel from the catalyst layers. The reaction sites where the catalyst, ionomer and reactants meet are crucial for efficient water splitting. Too much ionomer results in blocking of pores and high mass transport resistance. Too little ionomer or poor connectivity between them results in low proton conductivity.[40] The right amount and homogeneous distribution of ionomer in the catalysts is therefore important and necessary to maximize utilization of catalysts.

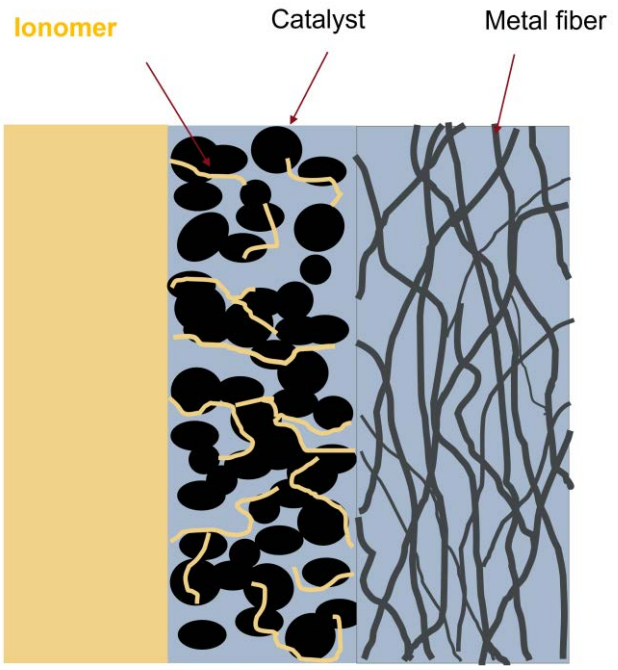

Figure 1-4 Schematic of a porous catalyst layer which sanwiched between PEM (left) and PTL (right) in water electrolysis cell.

1.3. PFSA and hydrocarbon ionomers

1.3.1. Traditional PFSAs and development of hydrocarbon ionomers

The industrial benchmark membrane material for PEM water electrolysis is Nafion®, a long side chain perflorosulfonic acid (PFSA) developed by DuPont since 1960.[41] Nafion® has a semi-crystalline polytetrafluoroethylene (PTFE) backbone with flexible perfluoroether pendant side chains terminated by sulfonic acid group (**Figure 1-5**). The PTFE backbone gives Nafion® excellent chemical stability, mechanical strength, and thermal stability. The dissimilar nature between backbone and ionic group tethered side chains gives Nafion® remarkable ion conductivity, typically when the membrane is hydrated.[23,42]

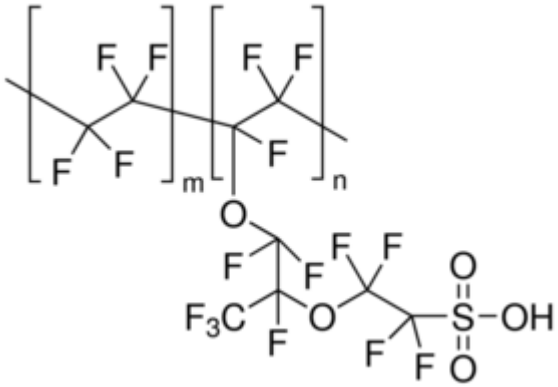

Figure 1-5 Chemical structure of Nafion, a perfluorosulfonic acid membrane where m =1 and n = 6-10.

Although Nafion® has been the technological and commercial benchmark for PEMs, its high cost (US$ 500 m^{-2}), environmental problems associated with the use of (per)fluorinated ionomers in mass production, limited operating temperature range (proton conductivity decreases at temperature over 100 ℃ due to dehydration) and high gas permeability (relatively high thickness (120-250 μm) are required to reduce gas crossover typical at high differential pressure (30 bar) for PEM water electrolysis operation), drives the need for a substitute. [2,5,11,43]

Hydrocarbon membranes are being considered as an alternative to traditional PFSA due to their potentially lower cost.[20,44] Additionally, this kind of PEM has several other advantages: appropriate conductivity, a better resistance than Nafion® to gas crossover, high glass transition temperature, and fewer environment concerns because the precursors are fluorine-free.[20]

Hydrocarbon membranes have been intensively studied for fuel cell applications.[5,45] Sulfonated polyethylene and sulfonated polyarylene were both initially attractive. However, it was found polyethylene-based ionomers are unstable in severe water electrolysis conditions (e.g. 80 to 100 °C) due to overheating and mechanical deformation.[46,47] In 1990s, Linkous and Slattery evaluated over 40 types of sulfonated polyarylene candidates and identified only a few options that could withstand elevated temperature of water electrolysis.[48,49] The sp^2 carbon in aryl-aryl and aryl-heteroatom linkages in the backbone of polyarylene is inherently stronger compared to sp^3 carbon in polyethylene such as sulfonated polystyrene. The inflexibility and bulky aromatic groups also give polyarylene higher glass transition temperature and less free volume for gas to permeate. Since then, the literature has been focused largely on sulfonated polyarylenes. Common examples (**Figure 1-6**) are polybenzimidazoles (PBI), poly(ether ether ketones) (PEEK), poly(ether sulfones) (PES) and polyphenyl quinoxaline (PPQ).[48,49,50]

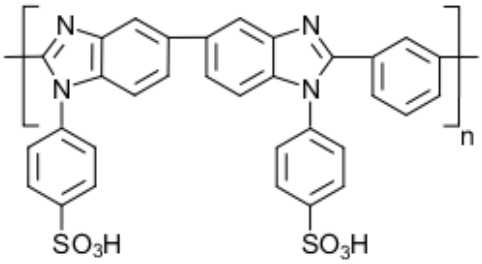

Sulfonated poly (benzimidazole)

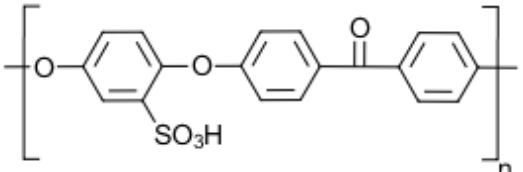

Sulfonated poly (ether ether ketones)

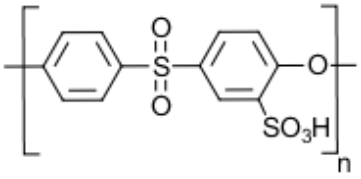

Sulfonated poly (ether sulfones)

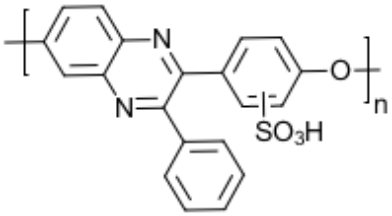

Sulfonated poly (phenyl quinoxaline)

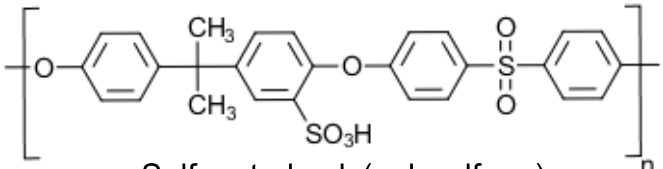

Sulfonated poly(polysulfone)

Figure 1-6 Representative sulfonated polyarylenes investigated for PEMWE.

1.3.2. Literature review of water electrolysis using hydrocarbon ionomers

There are many reports for PEM water electrolysis using PFSA as membrane and ionomer in the catalyst. Although different fabrication methods of MEAs and different testing facilities make it complicated to compare results from different groups, the general trends are similar. The polarization results (**Figure 1-7**) are typically between 1.53 to 1.8 V at 1 A cm^{-2} and 80 °C (See 2.4.1 for more about iV-curve).[4,9,51,52,53] Since early 2000 until now, only a few results report cell potentials below 1.6 V at 1 A cm^{-2}.[54,55,56] The cell voltage at a current density of 1 A cm^{-2} is a frequently taken metric to compare electrolysis results.

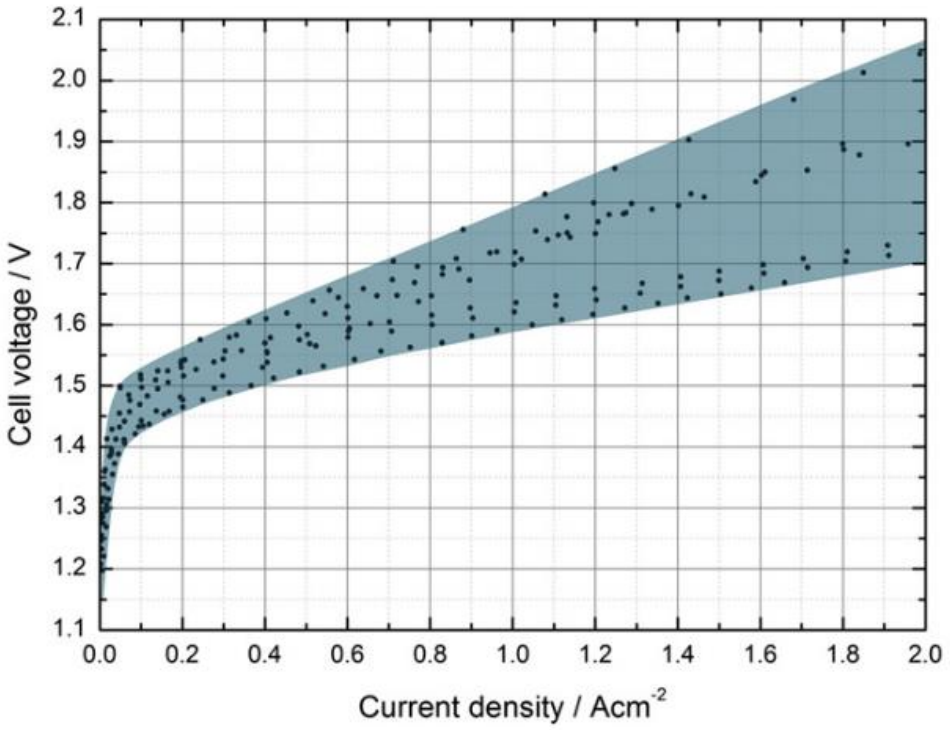

Figure 1-7 Performance range of published polarization curves from 2010 to 2012 for a PEM electrolysis single cell operating with Ir anode, Pt cathode, and Nafion® membrane at 80 °C. Reprinted with permission from reference 9. Copyright 2013 Elsevier Ltd.

Since the late 1990s, the application of hydrocarbon ionomers in water electrolysis has been explored. Linkous and coworkers reported water electrolysis using sulfonated poly (ether ether ketones) (sPEEK) as membrane with Ir as anode and Pt as cathode, achieving a current density of 30 mA cm^2 at 1.8 V, 60 ℃ .[50] Unfortunately, the

hydrocarbon-based ionomers suffered from excessive swelling in water at elevated temperature.[20] To reduce swelling, Jang et al. blended sPEEK and copolymer of sPEEK and sulfonated poly(polysulfone) (sPSf) with tungstophosphoric acid (TPA), respectively. The resulting blended membranes were electrical coated with Pt and gave voltages of 1.83 and 1.90 V respectively at 1 A cm^{-2} and 80 ℃ .[57] Recently, Siracusano and co-workers (2013) established a membrane-electrode assembly (MEA) using sPSf as membrane and Nafion® as ionomer in both IrO_2 and Pt/C catalyst layers and measured a cell voltage of 1.8 V at 1 A cm^{-2} and 80 ℃ .[58] In 2014, Skulimowska et al. reported sulfonated ether-linked polybenzimidazoles (sPBI) based MEA using IrO_2 and Pt as anode and cathode with Nafion® as ionomer in the catalyst layer, yielding a cell voltage of 1.71 V at 1 A cm^{-2} and 80 ℃ .[59] The introduction of ionomer in the electrodes greatly increased the utilization of catalysts and extended the reactions sites from 2-D to 3-D.

From the 1990s until now, most studies using hydrocarbon membranes used PFSA ionomer in the catalyst layer.[9] Wei et al. (2010) fabricated MEA using PES/sPEEK blended membrane using sPEEK in the catalyst layers. The voltage of this MEA which used Ir black and Pt/C as catalysts was 1.71 V at 1 A cm^{-2} and 80 ℃ .[46] Recently, Klose et al. introduced MEA consisted of poly (phenylene sulfone) (sPPS) as both membrane and ionomer achieving 1.62 V at 1 A cm^{-2} and 80 ℃ .[53]

Although efforts have been made to increase the efficiency of producing hydrogen using hydrocarbon membrane/ionomer in PEMWE. Only a few of the above-mentioned publications studied the stability of hydrocarbon membrane/ionomer in water electrolysis as hydrocarbon-based ionomers suffer from swelling and a great sensitivity to oxidative degradation compared to PFSAs, which have strong carbon-fluorine bonds.[20,60] Nolte et al. reported the lifetime of a partially sulfonated poly(arylene ether sulfone) for 300 h at a constant current hold of 1 A cm^{-2} (around 2.5 V) but at a relatively low temperature of 25 ℃ .[61] Siracusano et al. presented MEAs using sulfonated poly-sulfone (SPSf) as membrane and Nafion® as ionomer under a chronoamperometric test of 1.8 V (initially around 1.1 A cm^{-2}) and 80 ℃ for 32 h but did not report the evolution of current density.[58] Klose et al. performed durability analysis of a wholly sulfonated poly (phenylene sulfone) based MEA by holding current at 1 A cm^{-2} and 80 ℃ . The sPPS MEAs showed a voltage increase rate of 0.85 mV h^{-1}.[53] Further exploration of the stability hydrocarbon PEMs is therefore needed.

1.3.3. Sulfonated poly(phenylene)s

Sulfonated poly(phenylene)s which contain a fully aromatic backbone in **Figure 1-8** are considered to give inherent thermochemical stability compared to the labile heteroatomic linkage of other hydrocarbon ionomers and have gained particular interest as PEMs. However, the rigid-rod nature, especially for the entire *para* linkage type, makes it insoluble in common organic solvents and so polymerization of the backbone will terminate too early, resulting in precipititaion of the polymeric substrate and making high molecular weight difficult to reach.[22,62,63,64] Membranes prepared from the sulfonated hydrocarbon ionomers universally have high swelling values when hydrated in water, therefore poor mechanical properties, resulting in failure in fuel cell evaluations.

Functionalization of poly(phenylene)s backbone has been proposed to solve precipitation and increase the molecular weight.[65,66] C. H. Fujimoto *et. al.* reported sulfonated, phenylated poly(phenylene)s (sPPP) **(Figure 1-8)** using Diels-Alder synthetic method. This method benefitted from an inherent regiomeric imperfection and gives resulting ionomers appreciable solubilities in common organic solvents.[64]

The acid functionalization of sPPPs backbone is generally achieved by the post-sulfonation technique and the method has been followed for decades.[62] As the location and number of acid groups cannot be controlled, sPPPs synthesized from this technique suffer from ill-defined molecular structure, low solubility in polar solvent and uneven distribution of ionic groups.[60,62] These drawbacks limit their application in electrochemical devices.

The Holdcroft group demonstrated the synthesis of well-defined, branched sPPPs using pre-sulfonated monomer, which allows the precise positional control of sulfonic acid groups.[67] Membranes cast from this ionomer possessed high proton conductivity and oxidative stability.[67] sPPPs also showed comparable power density results as PEM and/or ionomer in the catalyst layer in *in situ* fuel cell tests compared to a traditional PFSA, which was unprecedented in the literature at the time for a chemically-stable hydrocarbon membrane.[67] sPPPs remain water-insoluble at RT, however it still exhibits excessive swelling and solubility problems in water at higher temperature, as with most hydrocarbon based ionomers, limiting *in-situ* durability.[60,67]

Recently, Adamski et al. reported a novel sulfonated phenylated polyphenylene sPPB-H^+ **Figure 1-8**.[60] By incorporating the spacer unit biphenyl in the ionomer backbone, the water solubility problem at evaluated temperature can be relieved. The membrane cast from sPPB-H^+ displayed excellent tensile strength, Young's moduli, and modest elongation at break.[60] It also revealed exceptional proton conductivities in both fully hydrated and reduced humidity in *ex situ* EIS test. For *in situ* fuel cell test, it displayed remarkable peak power density under non-optimized conditions and maintained high conductivity after 400 h accelerated stress testing with substantially lower H_2 gas crossover compare to benchmark Nafion 112.[60] Remarkably, it can dissolve in low boiling point organic solvent like methanol, giving it potential to be used as ionomer material in the catalyst layer.

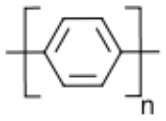

Poly (phenylene)

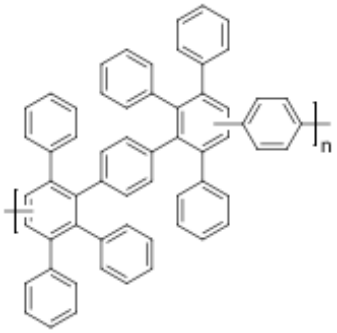

Phenylated poly(phenylene)

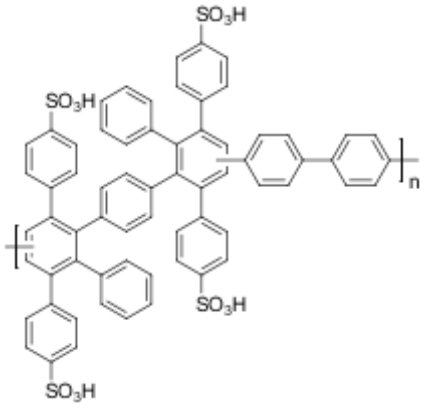

Sulfonated, phenylated poly(phenylene) biphenyl

Figure 1-8 The chemical structures of poly(phenylene) backbone, phenylated poly(phenylene) backbone and sulfonated phenylated polyphenylene with a biphenyl spacer unit.

1.4. Research objectives

This thesis research is focused on studying sulfonated phenylated polyphenylene sPPB-H^+ as a solid, proton conducting medium for water electrolysis. sPPB-H^+ is studied by firstly introducing it as the membrane and secondly by incorporating it as ionomer in the catalyst layers. The current-voltage characteristics of water electrolyzers based on sulfonated phenylated polyphenylene was investigated by I-V polarization curves and EIS. *Ex-situ* water uptake and proton conductivity of the PEM were also investigated to give insights into water electrolysis. The resistances hindering the efficiency of electrolysis cells based on these materials were identified with the help of electron microscopy.

Chapter 2.

Techniques and methods

2.1. Chemicals and apparatus

Chemicals used for fabrication of membrane electrode assemblies (MEAs) are given in Table 2.1. Equipment used is listed in Table 2.2.

Table 2-1 Membrane and catalysts

Chemical	Manufacturer
Nafion^{TM} 112	Du Point
Nafion^{TM} D520 dispersion (5 wt% in mixed alcohol)	Du Point
sPPB-H^+ membrane (50 ±2 μm)	-
sPPB-H^+ dispersion (3% w/v in MeOH)	-
Pt/C catalysts, 46.5% Pt	Tanaka Kikinzoku Kogyo
Ir black, 99.95%, 20-30 m^2 g^{-1}	Alfa Aesar

Table 2-2 Apparatus used for MEA fabrication and electrochemical measurements

Apparatus	Manufacturer
Electrolyzer test station (ETS)	Greenlight Innovation E20
5 cm^2 electrolyzer hardware	Fuel Cell Store
Potentiostat	Gamry Interface 5000
Airbrush	Paasche®
UP200Ht ultrasonic processor	Hielscher
Spray coater	Sono-Tek ExactaCoat
Scanning Electron Microscope	FEI Nova NanoSEM
Gas chromatography	Agilent 990 Micro GC

2.2. Ink preparation and electrode fabrication

MEAs were fabricated by spraying anode and cathode catalysts directly on the PEM surface. The preparation of catalyst inks using Nafion® as ionomer was shown as an example. The anode ink contained 2 wt% of solid (catalyst+ionomer) and 98 wt% of dispersing solvents (1:3 v/v water/IPA). The cathode ink contained 1 wt% of solid and the rest was dispersing solvent. Commercial Ir black and Pt/C were used as the anode and cathode catalysts, respectively. Catalyst ink was prepared in a glass vial: a desired amount of catalyst powder was firstly added, followed by adding Milli-Q water to completely wet the catalysts. Then, half of the required isopropyl alcohol (IPA) was added dropwise. The resulting slurry was sonicated in an ice bath to prevent overheating (Branson®) for 15 min. After that, Nafion D520 dispersion (5 wt% in mixed alcohol) was added dropwise to the vial. Finally, the other half of IPA was added to the vial to increase the total volume of the ink. The volume ratio between water and IPA was controlled as 1:3. The final ink was sonicated in an ice bath for additional 30 min to make a homogenous suspension and kept stirring before using.

The ink fabrication methods for both anode and cathode were the same. As unsupported Ir black settled faster than carbon supported Pt,[4] hand spray was employed to make anode electrodes using Paasche® airbrush. The use of airbrush avoided the loss of catalysts in the long tube of the machine sprayer (used for the cathode ink) as the paint cup was just next to the gun nozzle and allowed the spray small quantities of catalyst ink. For the anode, prior to hand spraying, the catalyst ink was additionally probe-sonicated (Hielscher UP200Ht) for 2 mins. Hand spraying was performed on vacuum hot plate (Welch™) at 90 ℃ (**Figure 2-1**). A PEM was framed with a transparent plastic sheet with 5 cm^2 opening to avoid overspraying. The spray path was controlled manually to be serpentine to ensure a uniform deposition on the 5 cm^2 area. For a 3.5 mg cm^{-2} loading of Ir, a total 3.5 mL to 4.5 mL ink was needed. As Ir can settles too rapidly, only 1 mL of ink was transferred from ink vial to spraying gun each time using a syringe. After completely spraying out 1 mL, another 1 mL was followed. All the anodes were controlled to have 3.5 ± 0.6 mg cm^{-2} loading of Ir.

The corresponding 1 wt% cathode catalyst ink was machine sprayed onto the other side of the membrane using an ExactaCoat (Sono-Tek) with integrated Contact Heating/Vacuum Plate (**Figure 2-2**). The deposition was operated at 80 °C under

vacuum. The inks were deposited on the membrane surface by a 120 kHz Ultrasonic Accumist Nozzle. To ensure uniform coating of the cathode, the spray pattern of the nozzle was programmed by Portal software. The flow rate was set as 0.25 mL min^{-1}. The shaping air pressure was adjusted at 0.8 kPa which is high enough to ensure that the spray was atomizing but not so high as to cause splashing. The path speed was 60 mm sec^{-1}. The loading of cathodes was around 1 mg cm^{-2} of Pt.

Figure 2-1 Vacuum hot plate (Welch™) used for hand spraying anodic catalyst layers; from left to right, components are digital temperature controller, vacuum hot table, three sheets of silicone rubber and vacuum pump.

For catalyst inks with sPPB-H^+ as the ionomer, a 3% w/v ionomer dispersion was initially prepared by dissolving the required amount of ionomer in MeOH. The preparation of catalyst inks using sPPB-H^+ as ionomer and electrode fabrication were the same as Nafion® as ionomer except the dispersing solvent changed from 1:3 v/v water/IPA to 1:3 v/v water/methanol due to increased solubility of sPPB-H^+ in methanol.

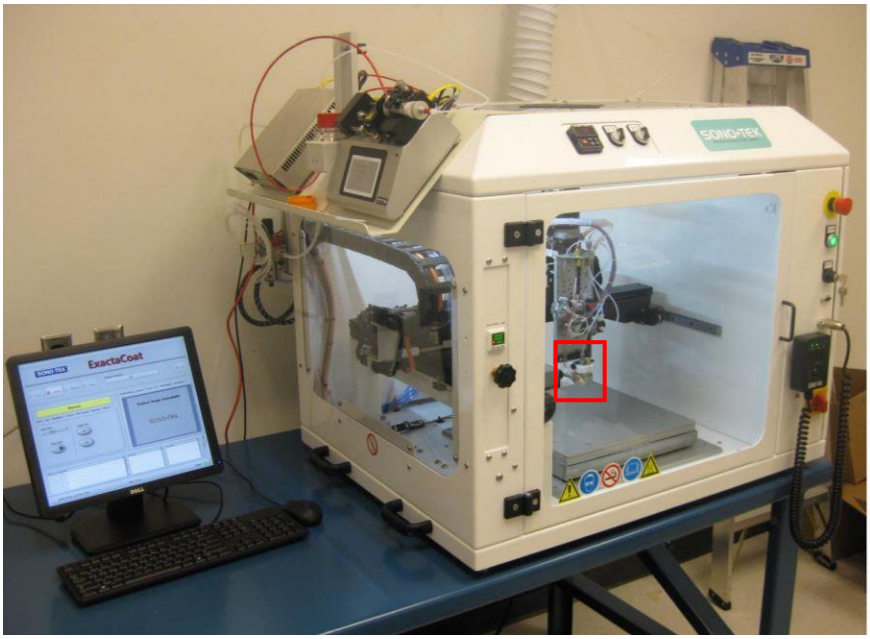

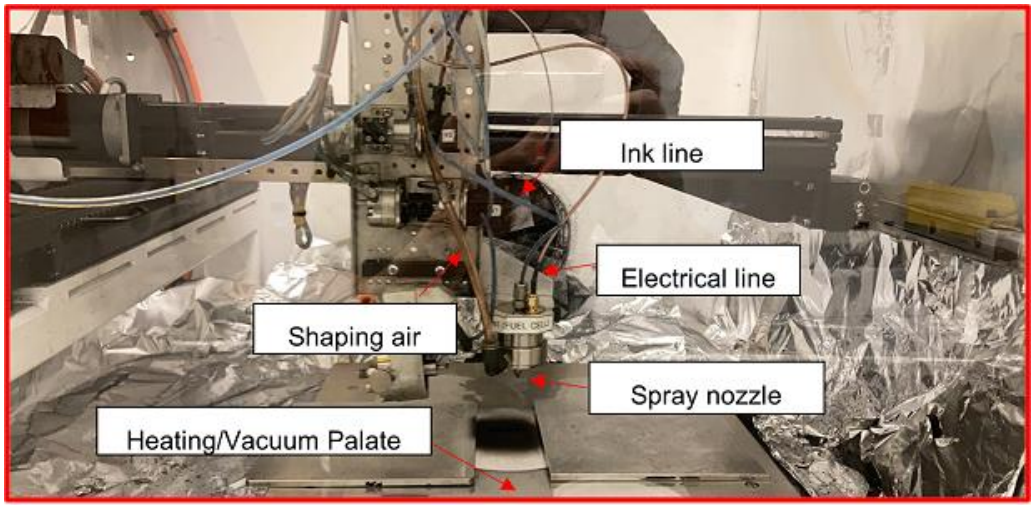

Figure 2-2 Spray coater (Sono-Tek) with main components labelled below used for automatic spraying cathodic catalyst layers.

2.3. Membrane electrode assemblies in PEMWE

Prior to PEMWE assembly, a pressure test was performed to ensure uniform compression on the sealing area. A pressure sensitive paper (Prescale, Fujifilm) was sandwiched in the middle of the cell. The cell was then tightened with a torque of 20 IN.LB. The pressure paper indicated sufficient compression of the cell (**Figure 2-3**).

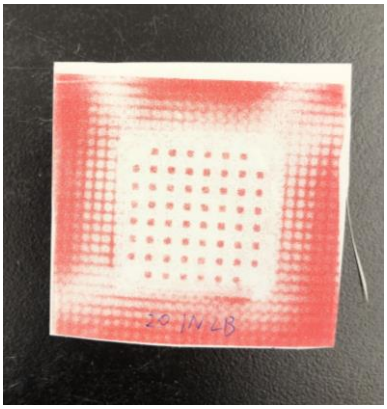

Figure 2-3 Sufficient and uniform compression on the sealing area of the cell.

Two Ti felts (ElectroChem.Inc) with 60% porosity and thickness around 0.270 mm were used as anodic and cathodic PTLs. The MEA and PTLs were sandwiched in Ti-based electrolysis cell housing (Fuel Cell Store Co.) and sealed by ice-cube polyolefin gaskets (QuinTech).

The detailed process of assembly of the sprayed MEA into the cell from outside inwards is shown in **Figure 2-4**. Each component needs to align well by hand with accuracy to make the most advantage, for example, the outer gaskets should not block the inlet/outlet for the water circulation and the inner gaskets should not cover the active area for the water splitting.

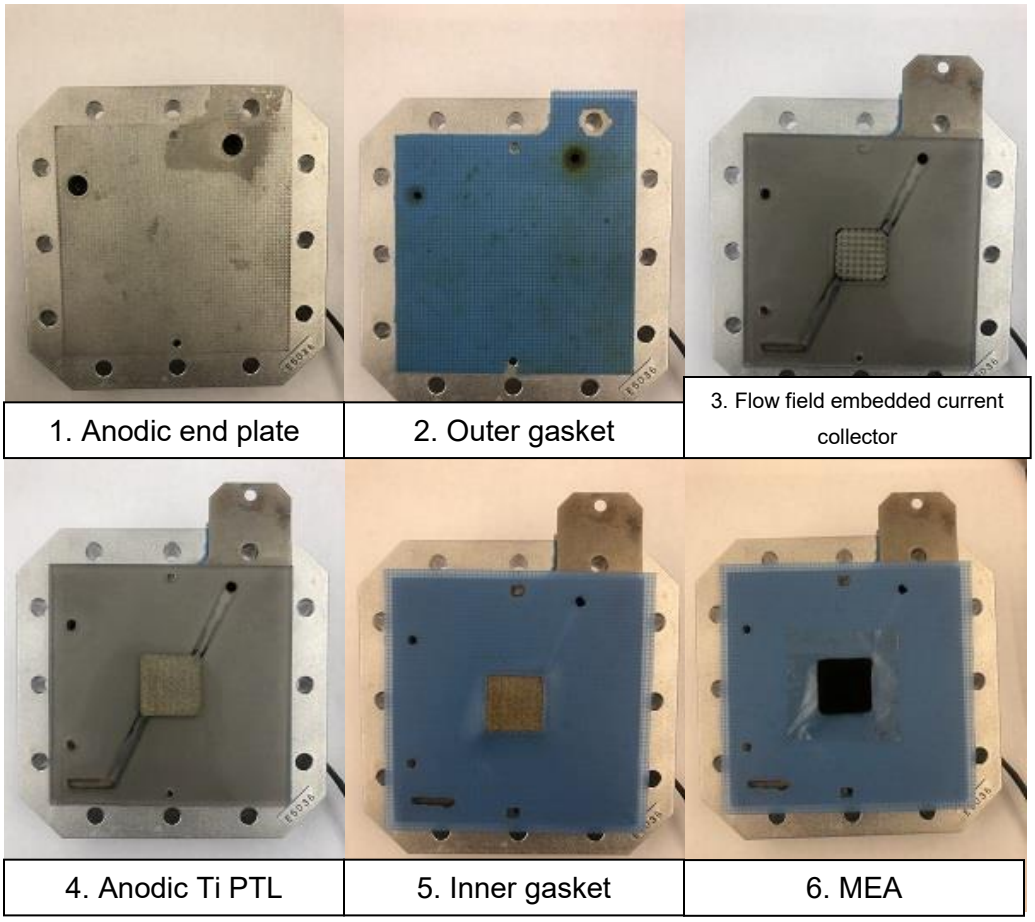

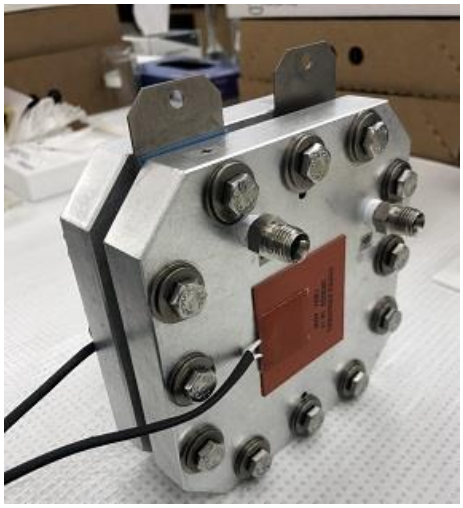

Figure 2-4 Pictures of cell assembly process of FuelCellStore water electrolyzer with a sprayed MEA. Components that need to be assembled from outside to inside are the anodic end plate, outer gasket, flow field embedded current collector, anodic Ti PTL, inner gasket and sprayed. Reversing the steps from 1 to 5 is the process for assemblying cathodic components.

2.4. Electrochemical measurements in the PEMWE

2.4.1. Polarization curves

Recording I-V polarization curves is the most common method in quantifying electrochemical systems under various conditions. Polarization curves are obtained either by controlling current and measuring the voltage or by applying voltage and measuring the current (the first method is preferred in this work). Current steps are performed in small increments and the responding voltage is measured until a steady state voltage is obtained (typically one minute for each increment if the cell is conditioned). All the polarization effects can be studied from cell potential behaviour including the reversible potential (1.23 V) and the irreversible overpotentials arising from activation, ohmic and mass transport losses against current density (**Figure 2-5**). As the cell components connected to each other in series, all the resistances and resulting overpotential from each electrode are summed to provide the cell polarization. A typical polarization curve can be separate into three distinct regions according to which overpotential dominates:[1,68,69]

- At low current density (0 A cm^{-2} to 0.3 A cm^{-2}), the water splitting reaction is activated and the charge transfer resistance (R_{CT}) at the anode and cathode dominates. Activation overpotentials arise from the inherent energy barriers for water splitting: HER at the cathode and OER at the anode. OER at the anode is much slower compared to HER at the cathode.

- At moderate current density (0.3 A cm^{-2} to 3 A cm^{-2}), the cell potential increases linearly with current density due to ohmic resistances. The ohmic resistance (R_{Ω}) is the sum of the electrical and ionic resistance. The electrical resistance is due to the metallic components of the cell (i.e., current collectors, flow fields, electrical wires and electrode materials) and interfacial electrical resistances (i.e., contact resistance between connections and PTLs/flow fields). The ionic related resistance includes membrane resistance, ionic resistance of the catalyst layers and interfacial resistance between the membrane and catalyst layers.

- At high current density (>3 A cm^{-2}), bubbles formed at electrode surface shield the active surface area and block the transport pathway of the water to the electrodes. Mass transport limitation caused by water starvation and bubble formation therefore becomes a significant source of performance loss.

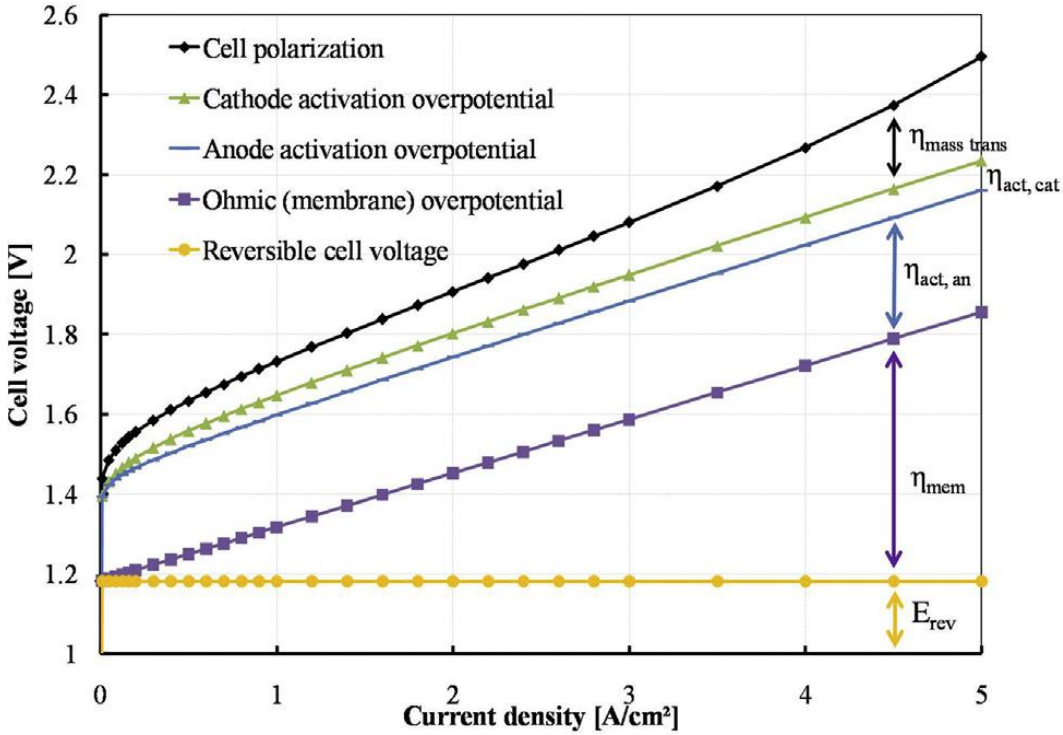

Figure 2-5 Example of PEM water electrolysis polarization curve including all the irrevisible losses to the cell polarization. Reprinted with permission from reference 68.Copyright 2017 Elsevier Ltd.

For this research, PEM electrolyzer cells were evaluated on a Greenlight Innovation E20 water electrolysis test station. Before electrochemical measurements on MEAs, the electrical resistance from the metallic hardware was determined. The electrical contribution from dry hardware resistance without assembling a membrane inside was measured to be between 20 and 40 mΩ cm^2 (potentiostatic EIS at 0 V with the AC perturbation at 10 mV) and monitored regularly (weekly) due to the gradual oxidation of the Ti PTL and flow field plates. If the hardware resistance was measured to be > 50 mΩ cm^2, new Ti PTLs were installed. If the hardware resistance was > 75 mΩ cm^2, etching of the flow fields was performed (**Appendix B**).

During water electrolysis, 200 mL min^{-1} of deionized water (18.2 MΩ) was fed through the anode and cathode compartments of the cell. Polarization data was

recorded by increasing the cell current stepwise from 0 mA cm^{-2} to 400 mA cm^{-2} in increments of 40 mA cm^{-2}. The step size was increased to 100 mA cm^{-2} up to 2.3 A cm^{-2}. 100 s stabilization period was programmed between each step. To protect the MEA, when the voltage approached 2.1 V, the increase of current density was terminated. The resulting stationary polarization curve was plotted using steady state currents and voltages.

2.4.2. Electrochemical impedance spectroscopy (EIS)

Ohm's law (equation 2.1) states the proportional relationship between current, I and voltage, V. The constant of proportionality is the resistance, R.

$$I = \frac{V}{R} \qquad \textbf{2.1}$$

This constant is also applied to alternating current. When a sinusoidal AC current I_t (Equation 2.2), involving the single frequency (f= ω/2π) is applied in an electrolyser, an alternating voltage output E_t (Equation 2.3) is obtained (**Figure 2-6**). As resistors (R), capacitors (C) and/or inductors (L) may be involved in a cell, the resulting voltage may not reach the amplitude peak at the same time as the current input and so the output will have a phase shift (ϕ). The phase shift for a pure resistor is zero.[70,71]

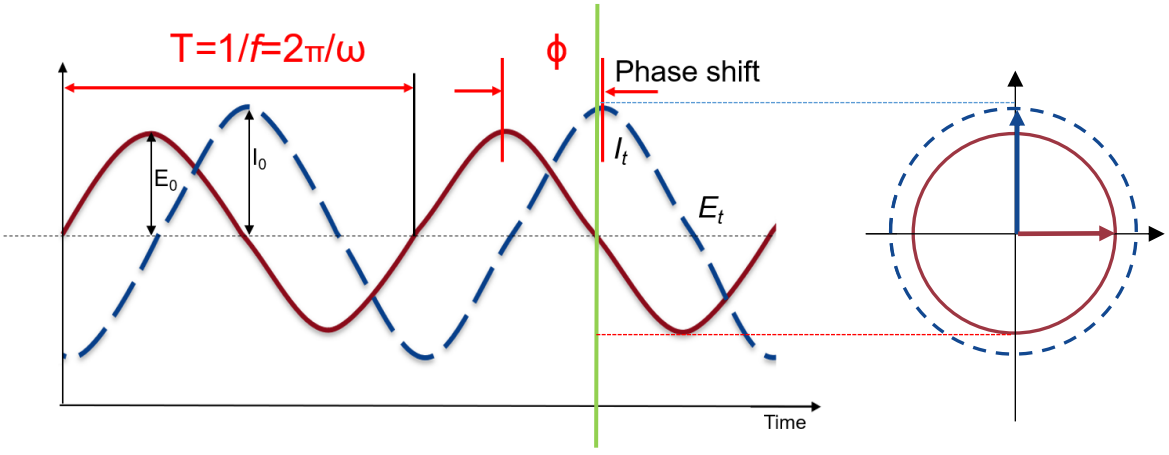

Figure 2-6 Sinusoidal current and potential response as a function of time, respectively.

Overall, the working principle of EIS is the study of impedance of an electrochemical system at different frequency when small perturbation is applied. When the frequency of the input changes, the processes occurring in the electrochemical system have different response time. [1,70,71,72]

Impedance is introduced as a vector diagram and complex number by C.P. Steinmetz and A.E. Kennelly, it has the real and imaginary part or alternatively it can be represented by absolute value and phase angle. The measurements of impedance over a range of frequency gives impedance spectrum — Nyquist plots and Bode plots (**Figure 2-7**).[70,71,73,74] In a Nyquist plot, the real and imaginary of an impedance can be easily identified. Bode plot displays the change of the magnitude and phase angle of the impedance over frequency.

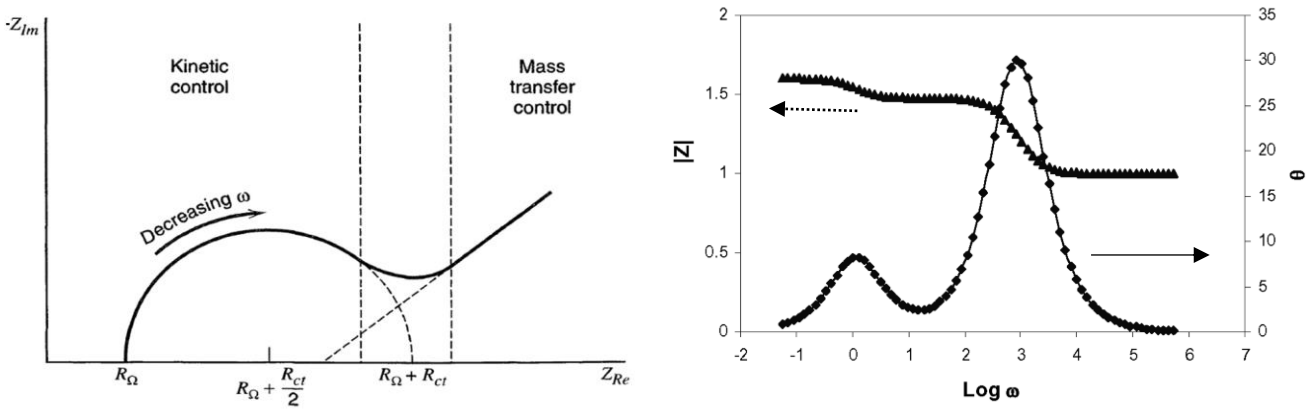

Figure 2-7 a) Nyquist plot and b) Bode plot of an electrochemical system. Reprinted a) with permession from 73.Copyright 2001 Wiley. Reprinted b) with permession from 74 .Copyright 2009 Springer-Verlag.

A Randles equivalent circuit is commonly used for interpretation of EIS Nyquist spectra for electrochemical systems. These circuits consist of an ideal constant phase ohmic resistance (R_Ω), a double layer capacitor (C_{dl}), a Warburg resistance (Z_w) and a charge transfer resistance (R_{CT}). A double layer capacitor (C_{dl}) and Warburg resistance (Z_w) is placed in parallel with a charge transfer resistance (R_{CT}). As HER and OER occur at separate electrodes for a water electrolysis cell, the equivalent circuit consists of two electrical components **(Figure 2-8)**. Usually, the double layer capacitance (C_{dl}) is replaced by a constant phase element (CPE) to model a nonuniform behaviour of a

double layer in the real word, for example due to the porous structure of electrodes.[75,76] When the frequency is very high, there is insufficient time for mass transport to equilibrate, which means Z_w, the diffusion process model will disappear. The impedance is charge transfer controlled as represented by the semi-circle in the Nyquist plot. When the frequency is low, the impedance is controlled by mass transport, shown as the tail in Nyquist plot. Z_w is difficult to isolate as it is always associated with C_{dl} and R_{CT}.[70,72] As the mass transport effect is not obvious for a laboratory scale water electrolysis cell, Z_w is removed. The simplified equivalent circuit (**Figure 2-9**) is used for analyzing impedance in this research.

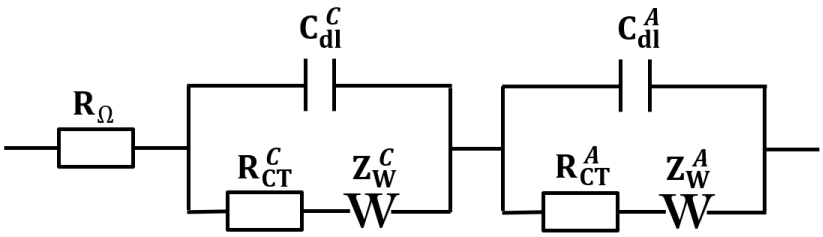

Figure 2-8 Scheme of an equivalent circuit for a water electrolysis cell.

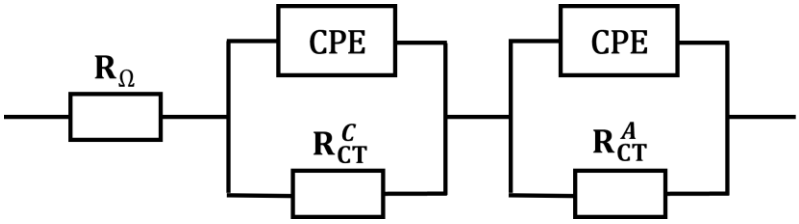

Figure 2-9 Equivalent circuit used to analyze the impedance data.

In the Nyquist plot (**Figure 2-7**), the high frequency intercept of semi-circles on x-axis is the ohmic resistance (R_{Ω})**.** The difference between R_{Ω} and low frequency intercept on x-axis is the charge transfer resistance (R_{CT}). Two semi-circles may be obtained to represent the faradic reaction on each electrode, or a single semi-circle may be seen as a merging response from both electrodes. The Nyquist plot can clearly distinguish between R_{Ω} and R_{CT} from the first sight. The characteristic frequency (top of the semi circle) can be calculated in equation 2.3:

$$\omega_{CT} = \frac{1}{R_{CT}C_{dl}} \qquad \textbf{2.3}$$

AC-impedance measurements (Gamry Interface 5000 potentiostat) between 100 kHz to 0.1 Hz were carried out at 100 or 700 mA cm^{-2}. The AC perturbation was

employed at 5% of the current input to obtain a sufficient signal to noise ratio, while keeping it small enough to ensure a linear system response.

2.4.3. Chronopotentiometry

The ability of a PEM water electrolysis cell to maintain its electrochemical efficiency over a significant period is a critical property for practical applications. A convenient way to evaluate the stability of a membrane electrode assembly in an electrolysis cell is to measure the time dependency of the cell voltage required for operation at a given current density. This technique is called chronopotentiometry. Chronopotentiometry was performed by holding the current density at 1 A cm^{-1} and at 70 °C. The corresponding voltage change for MEAs was monitored.

2.5. Scanning Electron Microscopy

Scanning Electron Microscopy (SEM) enables visualization of MEA cross-sections and catalyst layers. SEM is based on using a primary electron beam to probe the sample and the emitted secondary or backscattered electrons to form an image.[1] Using SEM helps determination of macroscopic features such as cracks in catalyst layers. SEM with Energy dispersive X-ray (EDX) spectroscopy was used to determine the elemental composition of electrodes. Scanning Electron Microscope (SEM) were performed at a voltage of 15 kV and a working distance around 7 mm. Cross sections of MEAs were prepared by cryofracture using liquid nitrogen and then investigated under SEM. SEM characterization was carried out on both freshly-prepared and used MEAs and electrodes.

2.6. *In-situ* gas crossover measurements

To test the hydrogen crossover through the PEM during electrolysis, *in-situ* gas chromatography (**Figure 2-10**) was used.[34,77] The moist anode gas was collected from the exhaust of Greenlight Innovation E20 PEM electrolyzer test station into a gas sampling bag. Before injecting the gas into an Agilent 990 Micro GC for analysis, the moisture of the anode gas was reduced using Drierite®. The anodic gas containing O_2 and H_2 is swept through a MGC CO_X column (1 m*0.8 mm ID) by Ar carrier gas and eluted to a thermal conductivity detector (TCD). The retention time of H_2 was

approximately 0.289 min and that of O_2 was 0.539 min. The H_2 in the mixture gas was calibrated using 2, 5.71 and 10 vol% H_2 in N_2 while the O_2 is calibrated using 99.998 % O_2. The example of Agilent report showing the separation of anodic gas and their calibration is attached in **Appendix A**.

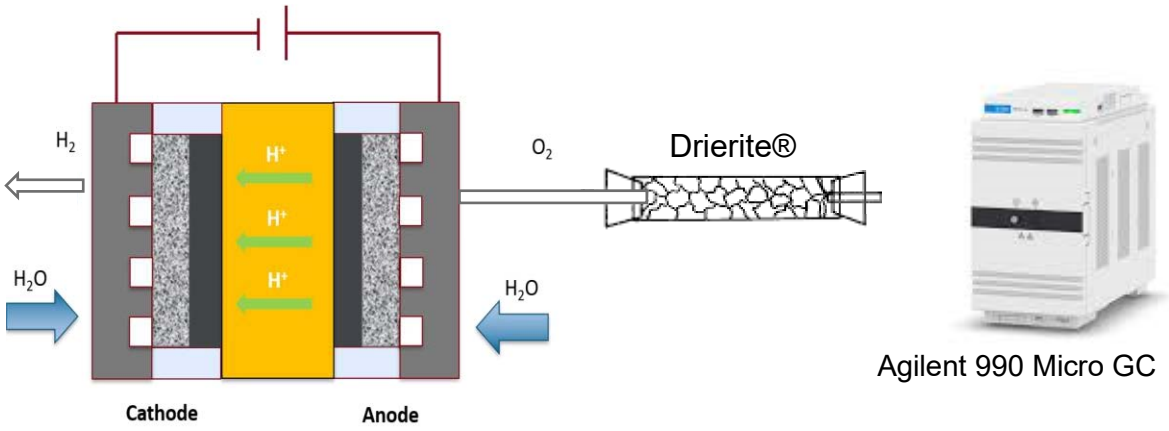

Figure 2-10 ***In-situ*** **gas chromatography test.**

2.7. Water uptake and dimensional swelling

The water uptake (ω) of the membrane was determined by a comparion of its fully dried and fully hydrated state. To make sure that the membrane was fully dried, the samples were placed in a vacuum oven at 80 °C for 24 h, cooled to room temperature under vacuum for 1 h, then the dry mass (ω_{dry}), out of plane thickness (Z_{dry}), in-plane area (A_{dry}) were immediately measured. After that, the samples were soaked in deionized water for 24 h, and the wet mass (ω_{wet}), wet thickness (Z_{wet}) and area (A_{wet}) were determined. The process were repeated for a minimum of three measurements per sample. The water uptake ratio by comparing the mass of a fully dried and fully hydrated membrane was shown in Equation 1.7 (reproduced here as Equation 2.3). The swelling ratio according to the area change was calculated using Equation 2.4.

$$\omega = \frac{\omega_{wet} - \omega_{dry}}{\omega_{dry}} \times 100\% \quad \textbf{2.3}$$

$$\text{Swelling ratio} = \frac{A_{wet} - A_{dry}}{A_{dry}} \times 100\% \quad \textbf{2.4}$$

2.8. Ex-situ proton conductivity test

Proton conductivity of PEMs was determined by placing a membrane sample (10 mm x 5 mm) into a conductivity cell containing Pt electrodes (**Figure 2-11**). Measurements were conducted under 95% RH at a defined temperature (using an Espec model SH241 humidity chamber) which is as close as practically possible to a fully hydrated state. The in-plane conductivity was measured by AC-impedance spectroscopy with a Solartron 1260 frequency response analyzer. The cell was subjected to a 100 mV sinusoidal ac voltage over a frequency of 10 MHz to 100 Hz, the impedance change of the cell at different frequencies was recorded as a Nyquist plot. The typical resulting Nyquist plot was evaluated using a Randles equivalent circuit (**Figure 2-12**).[78]

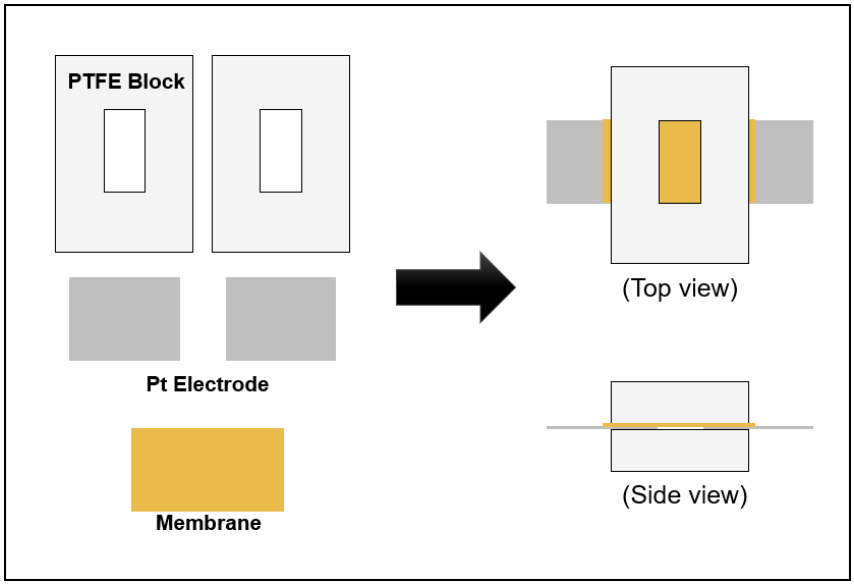

Figure 2-11 Schematic diagram of the conductivity cell incorporating two Pt electrodes.

As the lower limit of the frequency is 100 Hz, i.e., not enough time for mass transport to equilibrate, Warburg impedance (Z_w), which models the diffusion process, disappears. When the frequency approaches infinity, the impedance consists of the real component, which is the ohmic resistance (R_Ω) of the cell. As the Pt electrodes used have an electrical resistivity of only 10.87 μΩ cm at 300K, the ohmic resistance of the cell arising from the metallic resistance is low.[79] When the frequency is low, the overall circuit resistance is equal to the sum of the ohmic resistance (R_Ω) and the charge

transfer resistance (R_{CT}). The charge transfer resistance (R_{CT}) which then can be isolated as the diameter of the semi-circuit, represents electrolyte resistance (R_{el}) of the membrane. Proton conductivity σ $(\Omega \cdot cm)^{-1}$ was then calculated using Equation 2.5:

$$\sigma = \frac{L}{R_{el}A} \qquad \textbf{2.5}$$

where L (cm) is the distance between two electrodes, R_{el} (Ω) is the electrolyte resistance/the membrane ionic resistance and A (cm^2) is the cross-sectional area of the membrane.

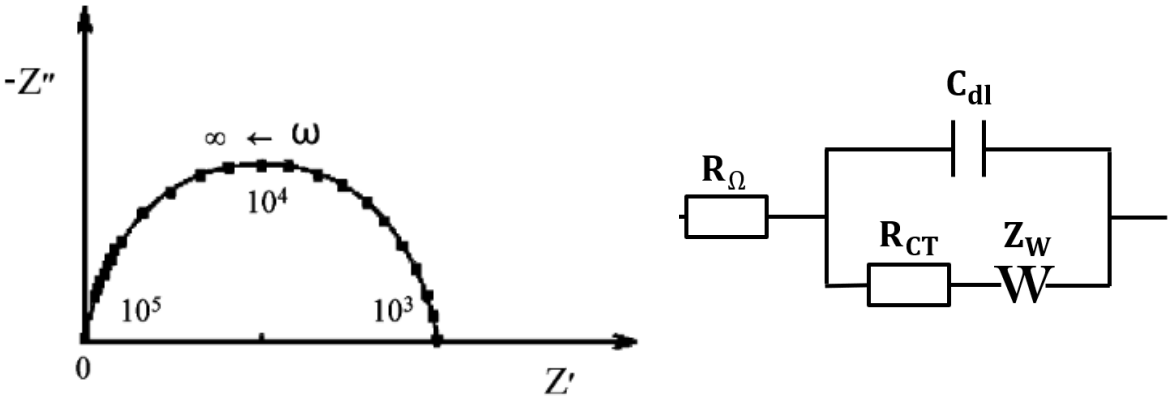

Figure 2-12 Typical Nyquist plot of conductivity cell (left) and a Randles equivalent circuit (right). Left picture reprinted with permission from reference 78.Copyright 2005 American Chemical Society.

Chapter 3.

PEM water electrolysis with hydrocarbon sPPB-H^+ as membrane and as the ionomer in the catalyst layers

3.1. Investigation of water electrolysis using sPPB-H^+ membrane

To study the characteristics of sPPB-H^+ hydrocarbon based ionomer in water electrolysis, MEAs were fabricated using sPPB-H^+ as the membrane and compared to those prepared with PFSA Nafion™ 112. The sPPB-H^+ membranes were cast with 50± 2 μm thickness to compare with Nafion™ 112 (51 μm). Nafion® binder was controlled at 10 wt% of Nafion in the anode and 20 wt% of Nafion in the cathode for all MEAs tested. MEAs were controlled with similar catalysts loading: 3.55 ± 0.65 mg_{Ir} cm^{-2} on the anode side of the membrane and 1.02 ± 0.11 mg_{Pt} cm^{-2} on the cathode.

The polarization curves and iR-corrected polarization curves for Nafion 112 based MEAs (red), and sPPB-H^+ membrane based MEAs (blue) are plotted (**Fig 3-1)**. At 1 A cm^{-2} (70 ℃), the voltage of all PFSA based (Nafion® used as both membrane and ionomer in catalyst layers) MEAs is in the range 1.74 - 1.77 V, in agreement with the state-of-art literature results (1.53 to 1.8 V at 1 A cm^{-2} and 80 ℃).[36] The electrochemical measurements are performed at 70 ℃ as the suggested operating temperature for the electrolyzer (FuelCellStore) is 35 ℃ to 75 ℃ . When catalyst layers are the same, sPPB-H^+ membranes (50 ± 2 μm) require a lower voltage than Nafion™ 112 at all current densities (1.70 vs. 1.75 V at 1 A cm^{-2}), which means less input energy is required to produce the same amount of hydrogen. The reproducibility of polarization curves for sPPB-H^+ membrane based MEAs is not as high as with Nafion 112 based MEAs, which may be due to the variation of membrane thickness during manual casting sPPB-H^+ membranes, as opposed to commercial roll-to-roll produced Nafion.

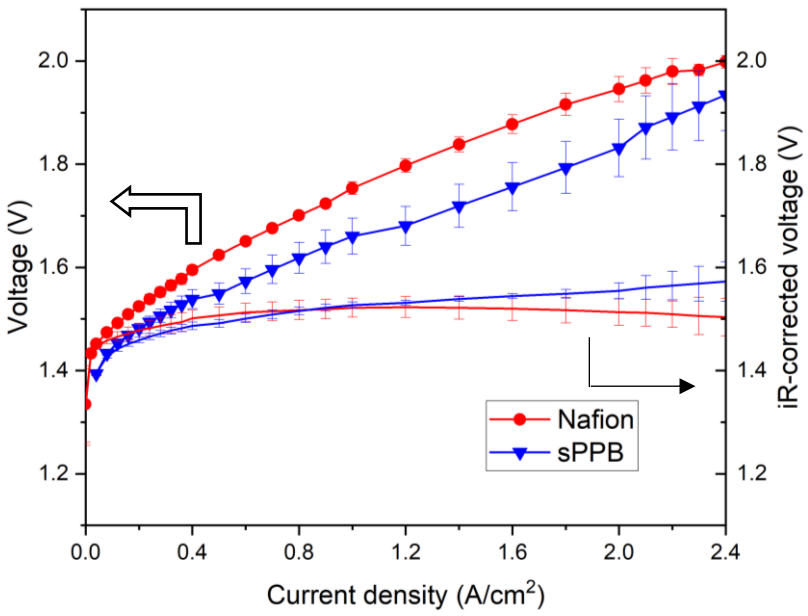

Figure 3-1 Polarization curves (line+symbol) and iR-corrected polarization curves (line) (70 ℃ , ambient pressure, 200 mL min^{-1} 18.2 MΩ deionized water) for Nafion 112 based MEAs (red) and sPPB-H^+ membrane based MEAs (blue). The error bars correspond to standard deviation between three measurements of identical samples. These MEAs contain ~3.5 mg_{Ir} cm^{-2}, 10 wt% Nafion® ionomer in anode and ~1.0 mg_{Pt} cm^{-2} 20 wt% Nafion® ionomer in cathode. The difference between MEAs is the membrane type.

Impedance measurements were carried out at two current densities: 100 and 700 mA cm^{-2}. At 100 mA cm^{-2}, the operation of the cell is under activation (kinetic) control, and so impedances are largely charge transfer resistances associated with catalytic activities. In contrast, at 700 mA cm^{-2}, impedances are more controlled by ohmic and mass transport limitations. As the catalyst layers in both MEA types are the same, the Nyquist plots (**Figure 3-2)** carried out at 700 mA cm^{-2} report on the effect of different membranes used in MEAs. The impedance data in this research was analyzed using an equivalent circuit (**Figure 2-9**) which contains R_Ω connected in series with two Randles circuit loops referring to the cathode and anode, respectively. R_Ω of sPPB-H^+ membrane-MEAs is 162 mΩ cm^2, 19.4% lower than the R_Ω for Nafion 112 based MEAs (201 mΩ cm^2). The charge transfer resistance (R_{CT}) for sPPB-H^+ membrane-MEAs (66.4 mΩ cm^2) is similar to that of Nafion 112 based MEAs (58.6 mΩ cm^2) proving consistency in the fabrication of catalyst layers.

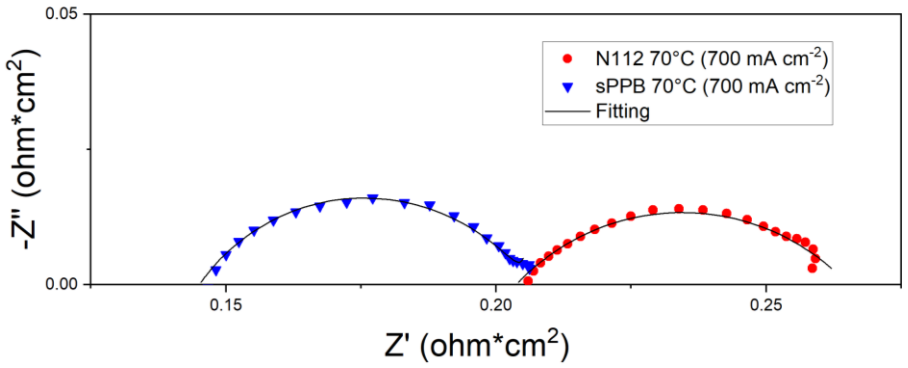

Figure 3-2 Nyquist plots performed at 700 mA·cm^{-2} and 70 ℃ for Nafion 112 based MEA (red) and sPPB-H^{+} membrane based MEA (blue). The average value and standard deviation between three measurements of identical samples are summarized in Table.1. These MEAs contain ~3.5 mg$_{Ir}$ cm^{-2}, 10 wt% Nafion® ionomer in anode and ~1.0 mg$_{Pt}$ cm^{-2} 20 wt% Nafion® ionomer in cathode. The difference between MEAs is the membrane type.

When the ohmic overpotential is subtracted from the overall cell voltage (using Ohm's law), the iR-corrected voltage is generated as a secondary vertical axis versus current. The iR-corrected voltage only considers the activation loss from the anode and cathode reactions and possible mass transport losses. The similar value of R_{CT} and iR-corrected voltages between Nafion 112 based MEAs and sPPB-H^{+} membrane based MEAs for current densities < 1 A cm^{-2} implies the main difference of performance between the two MEAs arises from a difference in R_{Ω}. The decreased R_{Ω} from the Nyquist plots therefore rationalizes the decreased voltage of sPPB membrane-MEAs compared to Nafion 112 based MEAs. Pertinent data extracted from polarization curves and EIS measurements are summarized in **Table 3-1**. sPPB-H^{+} membrane MEAs yield lower voltage (1.70 V) than Nafion 112 MEAs (1.75 V) at 1 A cm^{-2}. As discussed above, the voltage difference is due to much a lower R_{Ω} for sPPB-H^{+} membrane. As the electrical contribution was small (20 to 40 mΩ cm^{2}), the use of different membranes leads to different membrane/electrolyte resistance and interfacial resistance with catalyst layers, therefore, different R_{Ω}.

Table 3-1 Summary of the water electrolysis data extracted from polarization and EIS analysis of MEAs based on sPPB-H$^+$ and Nafion 112.

MEA	Ohmic resistance (R_Ω) @70 °C (mΩ cm^2)[a]	Charge transfer R_{CT}@70 °C, 700 mA·cm^{-2} (mΩ cm^2)[b]	Voltage @ 1A cm^{-2}, 70 °C[a]	R_Ω - corrected voltage @ 1A cm^{-2}, 70 °C[a]	Membrane conductivity (mS cm^{-1})[c]	IEC (meq g^{-1})[60]	Mobility @ 80 °C (10^{-3} cm^2 V^{-1} s^{-1})[60,80]
sPPB-H$^+$ (50±2 µm)	162±27	66.4±4	1.70±0.04	1.53±0.01	276±11	3.19	1.2
N112 (51 µm)	201±15	58.6±13	1.75±0.02	1.54±0.02	101±3	0.92	1.2

[a] From polarization data in Fig 3-1

[b] From intercept of real impedance axis in high frequency region of Nyquist plots data in Fig 3-2

[c] In-plane membrane conductivity measured *ex-situ* at 70 °C and 95% RH according to refs 30

To investigate the reason for the different *in-situ* R_Ω obtained from water electrolysis, ion exchange capacity (IEC), *ex-situ* proton conductivity (**Table 3-1**) for sPPB-H$^+$ membrane and Nafion™ 112 were measured. The lower *in-situ* R_Ω obtained from the water electrolysis measurements corresponds to a larger *ex-situ* conductivity of sPPB-H$^+$ membrane compared to Nafion™ 112 (276 mS cm^{-1} vs. 101 mS cm^{-1}). According to equation 1-6, the proton conductivity [σ, (S cm^{-1})] in a PEM is influenced intrinsically by IEC and the mobility of protons in a ionomer. The proton mobility in sPPB-H$^+$ is similar to PFSA membrane at relatively high temperature (i.e., 80 °C)[60,80]. The proton transport channel in Nafion® is bigger and has good connectivity as the dissimilar nature between hydrophobic PTFE backbone and hydrophilic acidic side groups. Though the phase separation of sPPB-H$^+$ is not as good as Nafion®, high water content of sPPB-H$^+$ as the high IEC by chance gives them the same conductivity at 80 °C. The proton conductivity in sPPB-H$^+$ is larger (276 mS cm^{-1} vs. 101 mS cm^{-1}) as a result of its much higher IEC, i.e., a higher concentration of charge carriers.

3.2. Wholly hydrocarbon sPPB-H$^+$ based PEMWE cell

3.2.1. Effect of sPPB-H$^+$ loading in anode catalyst layers

In addition to ionic conductivity of the PEM, the cell energetic efficiency depends on other factors such as catalyst loading, electrode binder content, or fabrication process of MEAs.[81] The ionomer content in the anode and cathode also needs to be optimized when new materials are introduced. To study the influence of sPPB-H$^+$ ionomer in the anode, MEAs were fabricated with catalyst layers with various amounts of sPPB-H$^+$ in the anode and a controlled sPPB-H$^+$ content in the cathode (15% relative to the total mass of cathode electrodes). The polarization curves of MEAs with an sPPB-H$^+$ content of 5, 10, 15, 20, 25 wt% in anode catalyst layer are plotted (**Figure 3-3**). The highest performance is obtained with 20 wt%, where a cell voltage of 1.90 V at 1 A cm^{-2} is achieved.

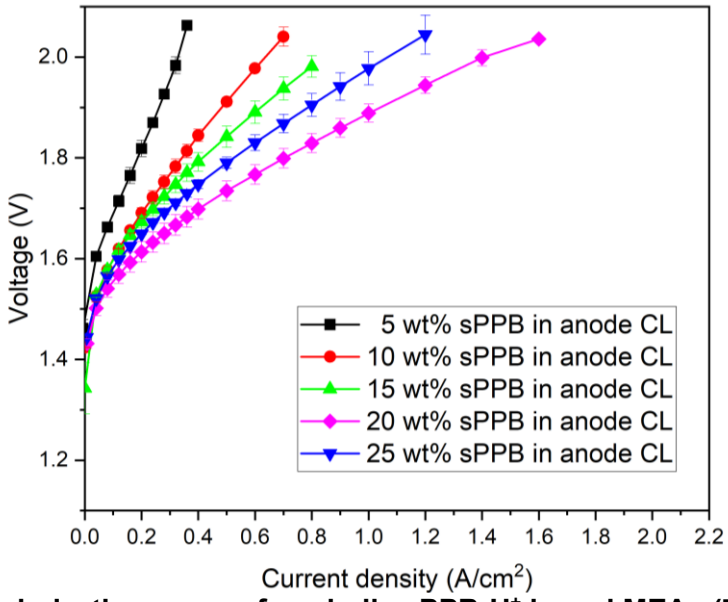

Figure 3-3 Polarization curves for wholly sPPB-H$^+$ based MEAs (70 ℃ , ambient pressure, 200 mL$_{H_2O}$ min^{-1}) with different weight percent of ionomer in the anodic catalyst layer. These MEAs contain ~3.5 mg$_{Ir}$ cm^{-2} and ~1.0 mg$_{Pt}$ cm^{-2}, 15 wt% sPPB-H$^+$ in cathode, and a 50 µm sPPB-H$^+$ membrane.

The Nyquist plot for these MEAs recorded at 100 mA cm^{-2} and 70 °C are shown in **Figure 3-4** and are fitted using an equivalent circuit (**Figure 2-9**). 100 mA cm^{-2} was chosen because at this current density, the operation is under activation (kinetic) control

and so the catalytic process related to ionomer content can be better analyzed. There are three semi-circles for the low anodic ionomer content (5, 10, and 15 wt%). When the ionomer content is increased to 20 and 25 wt%, the third semi-circle at low frequency disappears. The first two semi-circles in all the cases fit well using the equivalent circuit that contains two Randles circuit loops associated with the reactions at each of the anode and cathode. The third (low frequency) semi-circle results from mass transport losses. As the decreases in diameter of first semi-circle with anode ionomer content, indicating a decreasing R_{CT} for the oxygen evolution reaction (OER) (**Figure 3-4 a**). Its characteristic frequency (top of the semi-circle) remains the same around 15800 Hz in Bode plots (**Figure 3-4 b**). It is found that the diameter of the second semi-circle attributed to hydrogen evolution at the cathode remains unchanged – which is consistent with the ionomer content being held constant in the cathode. However, it is found that the characteristic frequency of the second semi-circle shifts from 400 Hz to 6 Hz with the increasing anodic ionomer content as reported in **Table 3-2**. As yet, this is not explainable. In order to fully understand the EIS results, a reference electrode may need to be introduced into the experimental setup in order to provide more details. [72,82,83,84]

a)

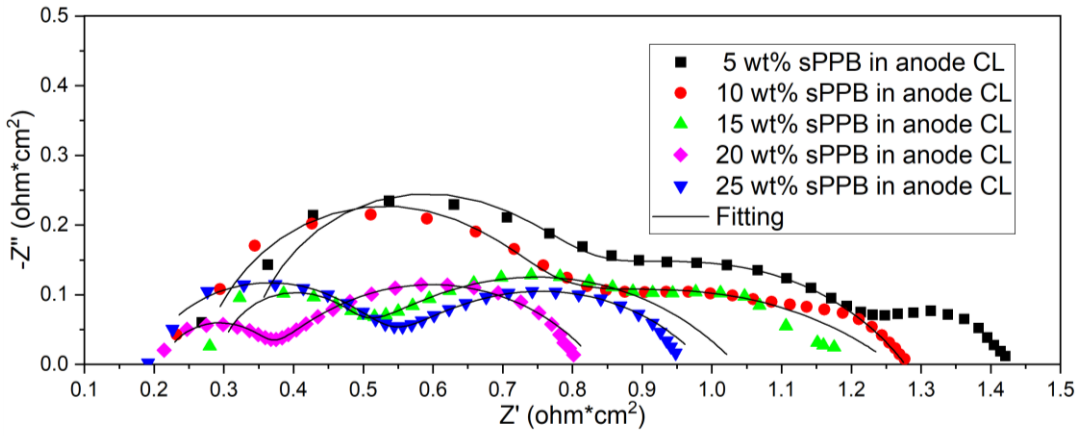

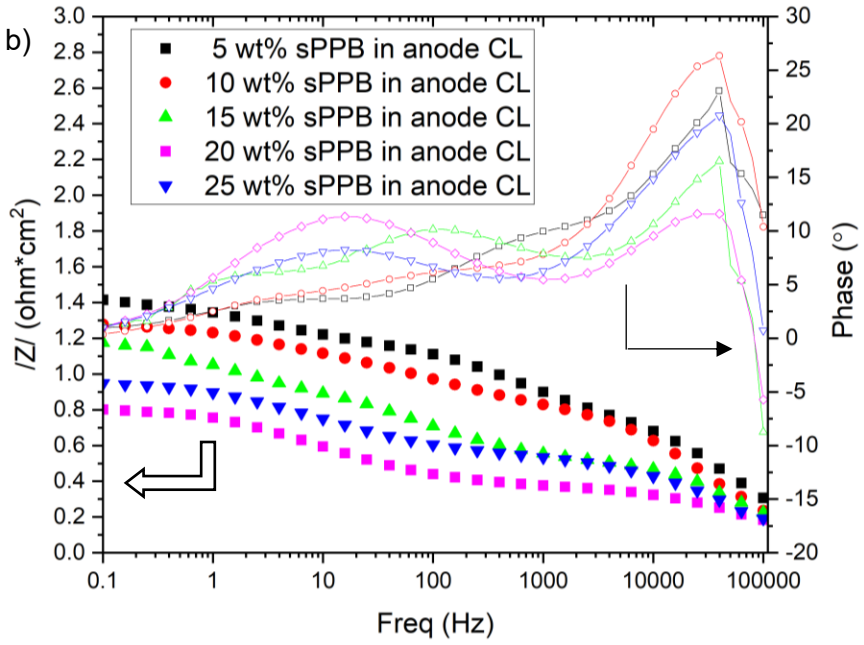

Figure 3-4 **Nyquist and Bode plots performed at 100 mA·cm^{-2} for wholly sPPB-H$^+$ based MEAs (70 ℃ 200 mL$_{H_2O}$ min^{-1}) with different weight percent of ionomer in the anodic catalyst layer. These MEAs contain ~3.5 mg$_{Ir}$ cm^{-2} and ~1.0 mg$_{Pt}$ cm^{-2}, 15 wt% sPPB-H$^+$ in cathode, and a 50 µm sPPB-H$^+$ membrane. The average value and standard deviation of samples are summarized in Table 3-2.**

As summarized in **Table 3-2**, R_{CT} for the OER decreases when ionomer content increases until the ionomer content reaches 20 wt%. MEAs with 5 wt% sPPB-H$^+$ in anode have the highest R_{CT} (967 mΩ cm^2), and this can be reduced to 793 mΩ cm^2 by lowering the ionomer content to 15 wt%. MEAs with a 20 wt% ionomer show the lowest R_{CT}, 629 mΩ cm^2. When the ionomer loading is increased 25 wt%, R_{CT} increases to 723 mΩ cm^2. R_Ω, is the largest for 5 wt% sPPB-H$^+$ ionomer content in the anodic electrode (319 mΩ cm^2). As ionomer content is increasing to 10 wt%, R_Ω decreases to 264 mΩ cm^2, and decreases to 200 mΩ cm^2 with further increases in ionomer content. It is noted that the lowest R_{CT} and R_Ω values are desirable in an PEMWE system. Therefore, the lowest impedance MEA corresponds to a 20 wt% sPPB-H$^+$ ionomer content in the anode. It is surmised that if the amount of incorporated ionomer is low, protons cannot fully access all the catalyst layer, leading to low catalyst utilization, and which explains the observation that 5 wt% sPPB-H$^+$ yields the largest R_{CT}.[37] A low ionomer content also means the continuity of the ionomer inside the catalyst layer is poor and that protons cannot sufficiently transport inside the catalyst layers and through the interface between the electrode and the membrane, resulting in a high R_Ω.[38,40] Excessive ionomer content,

however, can block the pores in the catalyst layer and cover too much surface of the catalyst, which is why 25 wt% sPPB-H^+ content yields the higher R_{CT} compared to 20 wt%.

Table 3-2 Summary of the EIS for wholly-sPPB-H^+ based MEAs with different ionomer content in anode. sPPB-H^+ membrane, constant sPPB-H^+ loading in the cathode, variable sPPB-H+ loading in the anode.

Cathode content (%)	Anode content (%)	Ohmic resistance R_Ω @70 °C (mΩ cm^2)	Charge transfer R_{CT} @ 100 mA cm^{-2} 70 °C (mΩ cm^2)	Charge transfer $R_{CT,\ loop\ 1}$ @ 100 mA cm^{-2} 70 °C (mΩ cm^2)	Characteristic frequency $_{loop\ 1}$ (Hz)	Charge transfer $R_{CT,\ loop\ 2}$ @ 100 mA cm^{-2} 70 °C (mΩ cm+)	Characteristic frequency $_{loop\ 2}$ (Hz)
15	5	319±24	967±55	454±54	15800	513±1	400
	10	264±16	862±33	311±4		551±29	100
	15	200±14	793±9	199±17		594±8	40
	20	196±18	672±40	172±31		486±14	10
	25	202±13	761±42	255±26		506±16	10

3.2.2. Effects of sPPB-H+ loading in cathode catalyst layers

In this section the anode ionomer loading on a sPPB-H^+ membrane was kept constant (20 wt% sPPB-H^+) and the cathode ionomer loading was varied from 15 to 30 wt% sPPB-H^+. Polarization curves of MEAs with 15, 20, 25, and 30 wt% cathode content are overlayed in **Fig 3-5.** The best performance is obtained with 20 wt%, where the cell voltage was 1.83 V at 1 A cm^{-2} and 70 ℃ .

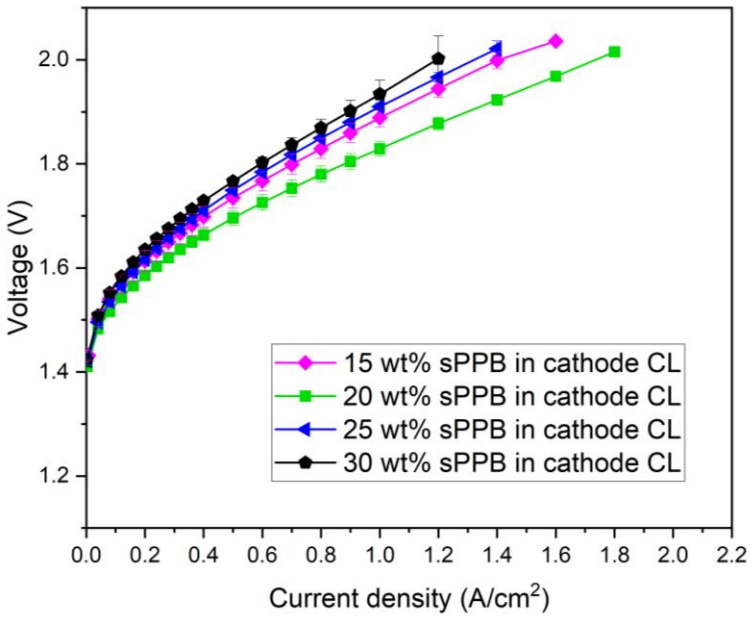

Figure 3-5 Polarization curves for wholly sPPB-H^+ based MEAs (70 °C, ambient pressure, 200 mL_{H_2O} min^{-1}) with different weight percent of ionomer in the cathode catalyst layer. These MEAs contain ~3.5 mg_{Ir} cm^{-2},20 wt% sPPB-H^+ in anode, and ~1.0 mg_{Pt} cm^{-2}, and a 50 µm sPPB-H^+ membrane.

EIS analysis of this series are presented as Nyquist plots and Bode plots in (**Fig 3-6**) and summarized in **Table 3-3**. Changing cathodic ionomer content fluctuates R_Ω value around 230 mΩ cm^2 and the characteristic frequency for cathode remains stable. The 20 wt% sPPB-H^+ in the cathodic electrode gives peak performance in polarization curves (i.e., lowest voltage) as R_{CT} is at its smallest (515 mΩ cm^2) (**Table 3-3)**. Decreasing or increasing cathodic ionomer content from this amount yields higher R_{CT}.

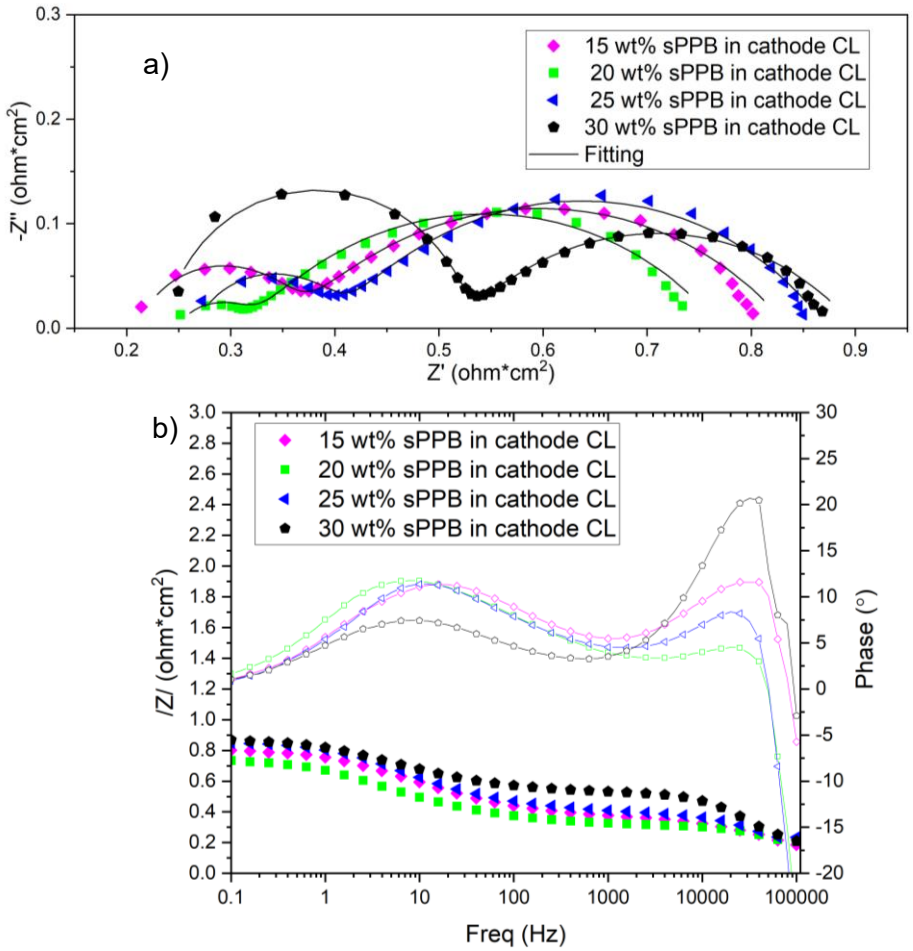

Figure 3-6 **a) Nyquist and b) Bode plots performed at 100 mA·cm^{-2} for wholly sPPB-H$^+$ based MEAs (70 °C, 200 mL$_{H_2O}$ min^{-1}) with different weight percent of ionomer in cathode catalyst layer. These MEAs contain ~3.5 mg$_{Ir}$ cm^{-2}, 20 wt% sPPB-H$^+$ in anode, and ~1.0 mg$_{Pt}$ cm^{-2}, and a 50 µm sPPB-H$^+$ membrane. The average value and standard identical samples are summarized in Table 3-3.**

Table 3-3 **Summary of the EIS all sPPB-H$^+$ based MEAs with different ionomer content in cathode.**

Cathode content (%)	Anode content (%)	Ohmic resistance R_Ω @70 °C (mΩ cm^2)	Charge transfer R_{CT} @ 100 mA cm^{-2} 70 °C (mΩ cm^2)	Charge transfer $R_{CT,\ loop\ 1}$ @ 100 mA cm^{-2} 70 °C (mΩ cm^2)	Characteristic frequency $_{loop\ 1}$ (Hz)	Charge transfer $R_{CT,\ loop\ 2}$ @ 100 mA cm^{-2} 70 °C (mΩ cm^2)	Characteristic frequency $_{loop\ 2}$ (Hz)
15	20	196±18	672±40	172±31	15800	486±14	10
20		244±5	515±11	75±4		439±16	
25		262±25	622±4	151±2		472±3	
30		226±23	672±6	285±22		387±16	

Chapter 4.

Chronopotentiometry and hydrogen gas crossover

Chronopotentiometry at a current density of 1 A cm^{-2} and 70 °C was performed on two sPPB-H^+ membrane based MEAs, two Nafion 112 based MEAs, and three wholly-hydrocarbon based MEAs using sPPB-H^+ as membrane and in the catalyst layers. The corresponding voltage change for MEAs with the different membrane but with Nafion® ionomer in the catalyst layer is plotted in **Figure 4-1**. The corresponding voltage change for wholly sPPB-H^+ based MEAs is plotted in **Figure 4-2**.

For sPPB-H^+ membrane MEA-1, the voltage increased 3.29 mV h^{-1} at 1 A cm^{-2} over the first 40 h. For sPPB-H^+ membrane MEA-2, the voltage increased 1.63 mV h^{-1} over the first 46 h. The voltages of sPPB-H^+ membrane MEAs both gradually increased to the point where the voltage became unstable and then dropped rapidly. For Nafion 112 MEA-1, the voltage was more stable, with an increase of 0.122 mV h^{-1}. For Nafion 112 based MEA-2, the voltage actually decreased 0.07 mV h^{-1}. In order to explain the latter, prior to chronopotentiometry, it is noted that each MEA had been conditioned for at least 40 min and underwent several electrochemical measurements (I-V polarizations and EIS at 70 °C, respectively). The decreasing voltage over 100 hours for Nafion 112 MEA-2 may arise from impurities in the catalyst layers being slowly flushed out during operation, exposing more active catalyst sites. For Nafion 112 MEAs, the degradation rate over 1000 hours is tens to hundreds of microvolt per hour according to testing conditions of different groups.[2,85] The degradation rate for sPPB-H^+ was significantly higher than for Nafion®. For sPPB-H^+ membrane MEA-2, chronopotentiometry was temporarily stopped at 3 h, 10 h, and 40 h in order to carry out electrochemical measurements (i.e., polarization curves and EIS). The Greenlight Innovation E20 water electrolysis test station (ETS) was shut down at 48 h for 20 min (without water and heat supply) as the pressure for the nitrogen for the safe purge was too low.

Chronopotentiometry (**Figure 4-2**) for sPPB-H^+ MEAs with 20 wt% sPPB-H^+ in both anode and cathode was investigated. The MEAs did not survive more than 5 h operation. From 0.5 h to 2 h, the voltage evolution rate for wholly- sPPB-H^+ based

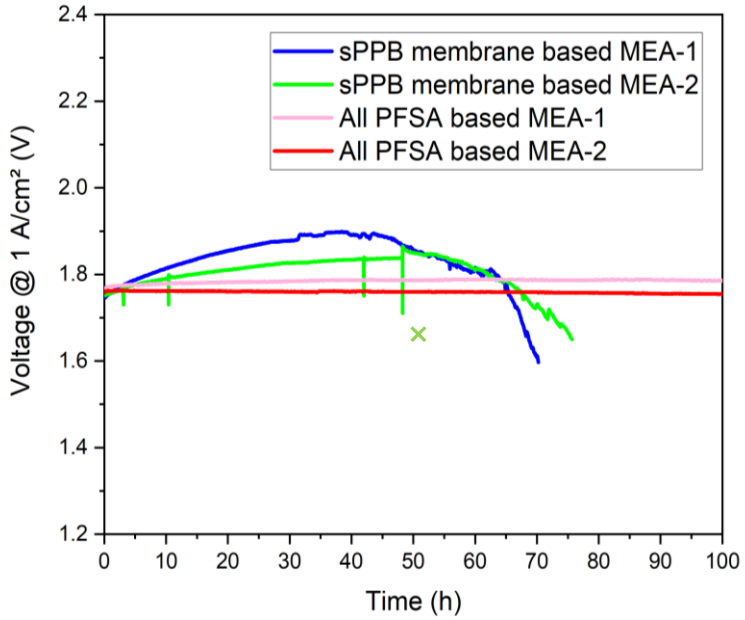

Figure 4-1 **100 h chronopotentiometry for two sPPB-H^+ membrane based MEAs and one Nafion 112 based MEA at 70 °C (200 mL_{H_2O} min^{-1}). These MEAs contain ~3.5 mg_{Ir} cm^{-2}, 10 wt% Nafion® ionomer in anode and ~1.0 mg_{Pt} cm^{-2} 20 wt% Nafion® ionomer in cathode. The difference between MEAs is the membrane type (× - ETS shut down for safe maintenance.**

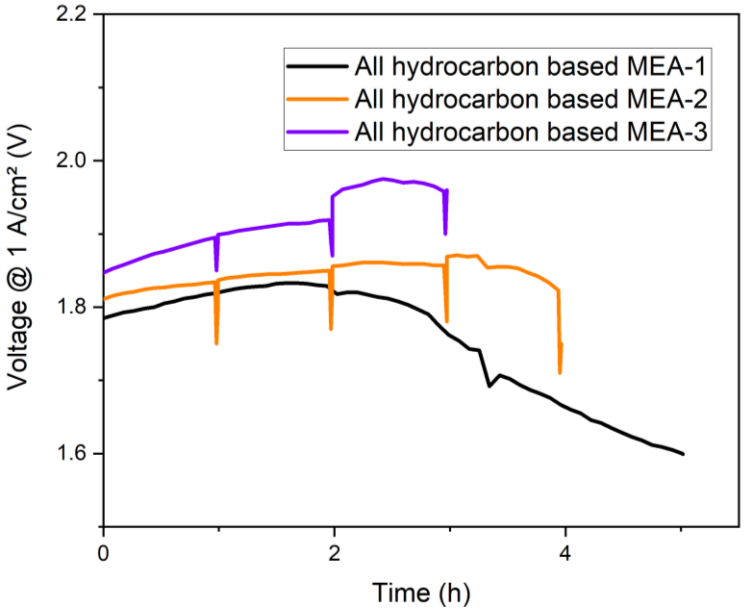

Figure 4-2 **Chronopotentiometry for three wholly-hydrocarbon based MEAs using sPPB-H^+ as membrane and in the catalyst layers at 70 °C (200 mL_{H_2O} min^{-1}). These MEAs contain ~3.5 mg_{Ir} cm^{-2}, 20 wt% sPPB-H^+ in anode and ~1.0 mg_{Pt} cm^{-2}, 20 wt% sPPB-H^+ in cathode, and a 50 µm sPPB-H^+ membrane.**

MEA-1 was 21.3 mV h^{-1}, for the wholly-sPPB-H^+ MEA-2, it was 17.3 mV h^{-1} and for MEA-3, it was 34.0 mV h^{-1}.

To analyze the increase of voltage in the early operating period (0-100 h), a 10 h chronopotentiometry measurement was carried out (**Figure 4-3 c**) for a sPPB-H^+ based MEA, and compared with a wholly- PFSA MEA. During the 10 h period, the voltage decreased 0.375 mV h^{-1} for Nafion 112 MEA-3 while the voltage increased 4.47 mV h^{-1} for sPPB H^+ based MEA-3. The polarization curves and EIS Nyquist plots before and after 10 h chronopotentiometry are compared in **Figure 4-3**. PFSA based MEAs appear stable according to both the polarization curves and iR-free polarizations before and after 10 h chronopotentiometry, as those curves are virtually overlapping. In contrast, sPPB-H^+ membrane MEA-3 reveals that iR-free voltages before and after chronopotentiometry shift, demonstrating that degradation arises not only from the membrane. Loss of activity of the catalyst can be observed from the increase of activation overpotential in the low current density range from the polarization curve. R_{CT}, determined by EIS, did not change; however, the faradic reactions from both electrodes became more distinguished after 10 h (**Figure 4-3 b**). The R_Ω increased from 178 to 243 mΩ cm^2 after 10 h operation. The substantially increased R_Ω indicated the increase of voltage shown in **Figure 4-1** is largely caused by the rise of R_Ω.

There can be two mains for the increase of R_Ω: an increase in electrical resistance or an increase in ionic resistance. The increase of electrical resistance is caused by surface oxidation of electrical components, especially on the anode side. Ionic resistance increases from a decrease in membrane conductivity and/or delamination between the electrode and membrane. The effect of metallic oxidation is not apparent over a 100 h chronopotentiometry analysis as surmised from the observation that the ohmic resistance for Nafion MEA did not change. However, passivation of Ti flow fields became noticeable after several chronopotentiometry studies (**Appendix B**). Loss in membrane conductivity could result from contamination by multivalent ions (e.g., iron and nickel) released from the ETS stainless steel connections. The conductivity of circulated water before and after the long-time chronopotentiometry was therefore measured and compared (**Appendix C**).

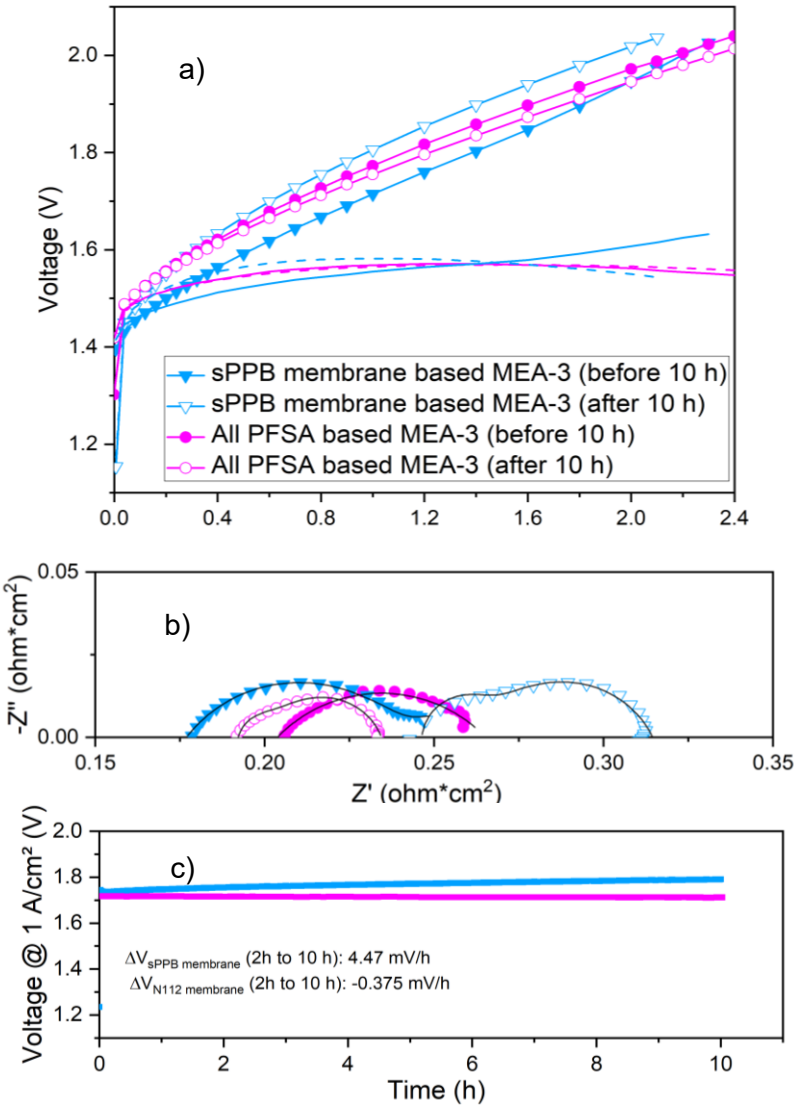

Figure 4-3 **a) Individual polarization curves (line+symbol) and iR-corrected cell voltage verse current density [before (solid line) and after (dash line) 10 h chronopotentiometry], b) Nyquist plot performed before (solid symbols) and after (empty symbols) 10 h chronopotentiometry at 700 mA·cm^{-2}, c) 10 h chronopotentiometry for one Nafion 112 based MEA and one sPPB-H$^+$ membrane based MEA (70 °C, ambient pressure, 200 mL$_{H_2O}$ min^{-1}). These MEAs contain about 3.5 mg$_{Ir}$ cm^{-2} (10 wt% Nafion® ionomer) on anodic side of the membrane and 1.0 mg$_{Pt}$ cm^{-2} (20 wt% Nafion® ionomer). The difference between the MEAs is the membrane type.**

For Nafion 112 MEAs, the increase of conductivity for the circulated water for both electrodes was negligible: the conductivity of anodic circulation increased from 0.60 to 0.76 μS cm^{-1} while the conductivity of cathodic circulation water increased from 0.56 to 0.62 μS cm^{-1}. For sPPB-H$^+$ membrane MEAs using Nafion® in the catalyst layers,

conductivity value for the anodic circulation water after chronopotentiometry study increased slightly over time. The conductivity of the anodic circulation water increased to 1.27 μS cm^{-1} from 0.44 μS cm^{-1} after 100 h chronopotentiometry test while the conductivity of cathodic circulation only increased to 0.65 μS cm^{-1} from 0.40 μS cm^{-1}.

The water conductivity for wholly-sPPB-H^+ MEAs after 5 h chronopotentiomety was also investigated and the conductivity of circulated water increased significantly (**Appendix C**). At the beginning, the conductivity of the deionized water for both anode and cathode was around 0.44 μS cm^{-1}. After 5 h circulation, the conductivity of water for the cathode was increased to 1.07 μS cm^{-1}. The water conductivity for the anode was over 7.25 μS cm^{-1}. From the three-layer cross-sections (**Figure. D3**) for wholly-sPPB-H^+ based MEA, Ir catalysts can hardly be found on the membrane surface after the chronopotentiometry. The precipitate of Ir can be found in anodic circulation water (**Figure. C1**) after chronopotentiometry study. Therefore, the increase of the water conductivity is caused by the catalyst delamination.

From the *ex-situ* dimensional change observed for different membrane after soaking in water for 24 h (**Table 4-1**), the thickness of sPPB-H^+ increased by 62.5% from 50 μm. The Nafion 112 membranes which initially had similar thickness like sPPB-H^+ increased only by 14.4% after soaking. Accordingly, for the *in-situ* water electolysis studies, delamination of the catalyst layer occurred due to swelling of sPPB-H^+ at the membrane/electrode interface, therefore the water conductivity of sPPB-H^+ membrane based MEAs was slightly higher than Nafion 112 MEAs. For wholly-sPPB-H^+ based MEA, the swelling occurred at the interface as well as inside the catalyst layers, the catalyst delamination was severe and significantly caused water conductivity increase.

One of the reasons for the increase of R_Ω is therefore from the reduced contact between the membrane and catalyst layers and the increased proton transport resistance inside the catalyst layer due to the loss of ionomer (**Figure 4-3 b** and **Figure 4-4**). Due to the lack of ionomer as the binder to secure the catalyst particles, R_{CT} also increases.

Table 4-1 **Dimensional changes of proton exchange membranes (ca. 2*2 cm, 50 μm) from ambient to fully hydrated (equilibrated in DI H2O for 24 h) states at room temperature and 70 °C, respectively.**

Membrane	Area[a]$_{room\ T}$ (%)	Thickness[b]$_{room\ T}$ (%)	Water uptake ratio[c]$_{room\ T}$	Area$_{70\ °C}$ (%)	Thickness$_{70\ °C}$ (%)
sPPB-H+	16.4±0.4	62.5±1.8	78.1±3.3	42.0±1.3	103±3
NR-112	6.1±0.7	14.4±1.7	13.7±0.4	25.2±2.4	36.4±1.8

[a] In-plane (XY) area [b] Out of plane (Z) thickness [c] Water uptake ratio=$\frac{m_{wet}-m_{dry}}{m_{dry}}$

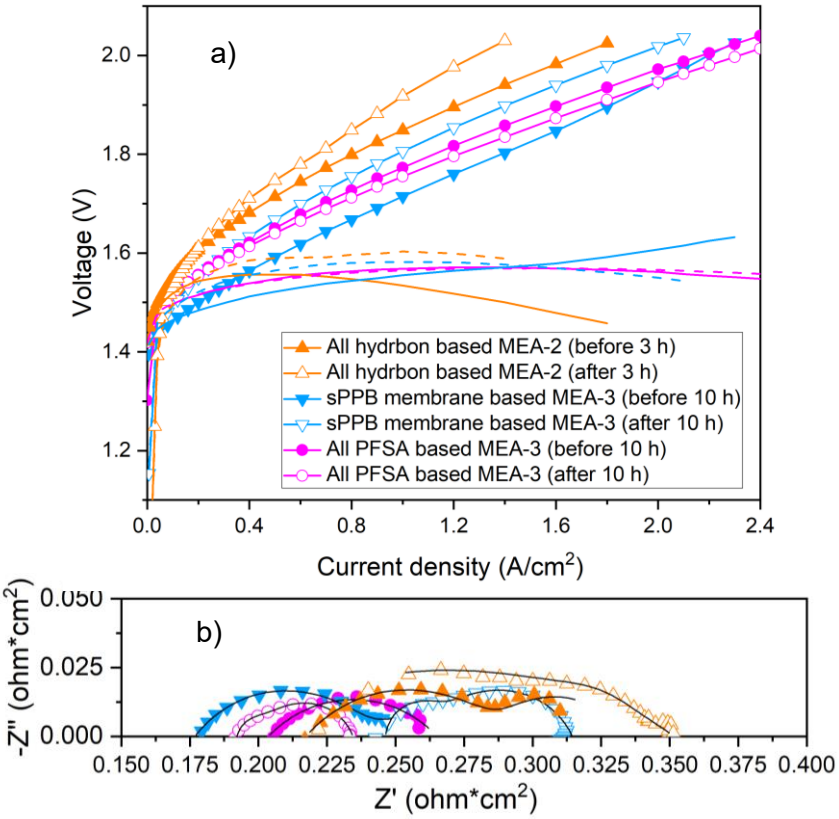

Figure 4-4 **a) Individual polarization curves (line+symbol) and iR-corrected cell voltage verse current density [before (solid line) and after (dash line) long time chronopotentiometry], b) Nyquist plot performed before (solid symbols) and after (empty symbols) chronopotentiometry at 700 mA·cm^{-2} for wholly-sPPB-H$^+$ based MEAs (70 °C, ambient pressure, 200 mL$_{H_2O}$ min^{-1}). The MEA contains about 3.5 mg$_{Ir}$ cm^{-2}, 20 wt% sPPB-H$^+$ in both anode and cathode. (Polarization curves and EIS for wholly-sPPB-H$^+$ based MEA is plotted with that of sPPB-H$^+$ membrane based MEA and Nafion 112 based MEA to make a direct comparison.)**

The gaseous exhaust of the anode during chronopotentiometry (@ 1A cm^{-2}) for different MEAs was collected to analyze *in-situ* hydrogen gas crossover into the anode compartment (i.e, contamination of electrochemically generated oxygen) (**Figure 4-5**). Initially, at 1 A cm^{-2}, wholly-Nafion ionomer MEA yields a hydrogen crossover of 1.10 vol% in oxygen, and stabilizes at that value. For sPPB-H^+ membrane MEAs (Nafion® as ionomer), H_2 gas crossover is reduced (0.55 vol%). Wholly-sPPB-H^+ MEAs yield an even lower H_2 gas crossover of ~ 0.4 vol%. However, the low gas crossover was not stable. For the sPPB-H^+ membrane MEAs-2, the hydrogen in oxygen at 1 A cm^{-2} increased almost linearly from 0.58 to 1.17 vol% for the first 40 h. For wholly-sPPB-H^+ MEAs, gas crossover is >1 vol% after only 3 hours of chronopotentiometry.

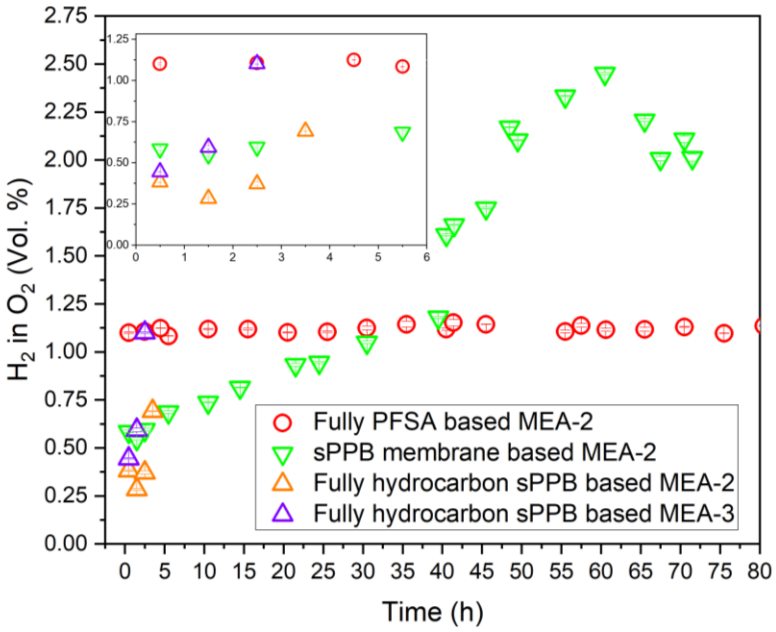

Figure 4-5 In-situ measurements of anodic hydrogen crossover using gas chromatography. The gas was collected at 70 °C at @ 1 A cm^{-2} from ambient pressure water electrolysis for wholly sPPB-H^+ based MEAs, a sPPB-H^+ membrane (Nafion D520 as ionomer) based MEA and a wholly PFSA based MEA.

As the dissolved gas can diffuse through water-filled channels in the electrolyte membrane.[34] The driving force is the differential concentration of dissolved gas in the liquid water across the membrane. Coinciding with an increase in hydrogen crossover in anode, increased oxygen in cathode is expected. The crossover of oxygen can lead to the electrochemical formation of hydrogen peroxide (H_2O_2) at the cathode side (0.68 V vs. RHE). Peroxide may decompose into free radicals in the presence of metal-ion

impurities which can lead to chemical degradation of the components.[86,87] As the cell voltage during chronopotentiometricy analysis reaches high positive values (> 1.7 V), chemical degradation of membrane by the radical attack becomes a possibilty. A gradual loss of membrane can also be one of the reasons for the increase of R_{Ω}**.** Moreover, chemical degradation may result in the formation of pinholes in the membrane, leading to the increased gas crossover. In turn, increased gas crossover through pinholes may also increase the contact resistance of the catalyst layer with the membrane, via delamination. Visual proof of delamination of the catalyst layer is presented in **Figure C2** in **Appendix C**.

As mentioned above, the current supplied to sPPB-H^+ membrane MEA-2 was interrupted at 3 h, 10 h and 40 h in order to perform electrochemical measurements and after 48 h to change the safely purge gas supply (**Figure 4-1**). A sharp increase of gas crossover was also found at 40 h and 48 h, and the MEAs became fragile, losing mechanical strength. The unstable and dropping voltage in the later part of the chronopotentiometry is also the result of increasing gas crossover. The permeated oxygen can combust with hydrogen near the cathode by Pt, creating hot spots affecting cell stability. The presence of oxygen at the cathode via gas crossover also leads to a parasitic current, giving the appearance of depolarization of the cell, analogous to “soft shorts”. [13, 88, 89]

A soft short is a term for an electrical short that does not cause immediate cell failure.[89] When a soft short arises in the system, the current first passes through the electrical short until the threshold water-splitting voltage is reached. Polarization analysis and EIS (**Figure 4-6 a and b**) were also performed at the end of chronopotentiometry study (75 h for sPPB-H^+ membrane MEA-2 and 100 h for Nafion 112 MEA-2). Wholly-PFSA MEAs were stable after 100-h chronopotentiometry. For the sPPB-H^+ membrane MEA, the cell polarization shows two slopes below and above 0.5 A cm^{-2} after 75-h chronopotentiometry. The steep slope at the region where the Nernst potential of water splitting not reached is caused by “soft shorts”.[88, 89] The occurrence of short circuit resistor is verified using a modified equivalent circuit to fit the EIS spectra (**Figure 4-6 c**). When the membrane is electrically shorted, a “damaged cell circuit” is used containing a short circuit resistor parallelly connected to a “normal cell circuit”. Initially, the current travels through the short circuit resistors. No gas generation occurs. When the water splitting voltage is reached, some of the current is used for faradic reactions for

producing hydrogen and oxygen while others are consumed as short-circuiting current. For MEAs in which membranes have not been short-circuited (Nafion 112 MEAs before and after chronopotentiometry and sPPB-H^+ membrane MEAs before chronopotentiometry), their impedance data fits well using a “normal cell” circuit, i.e., all the current flows through the electrolytic cell.

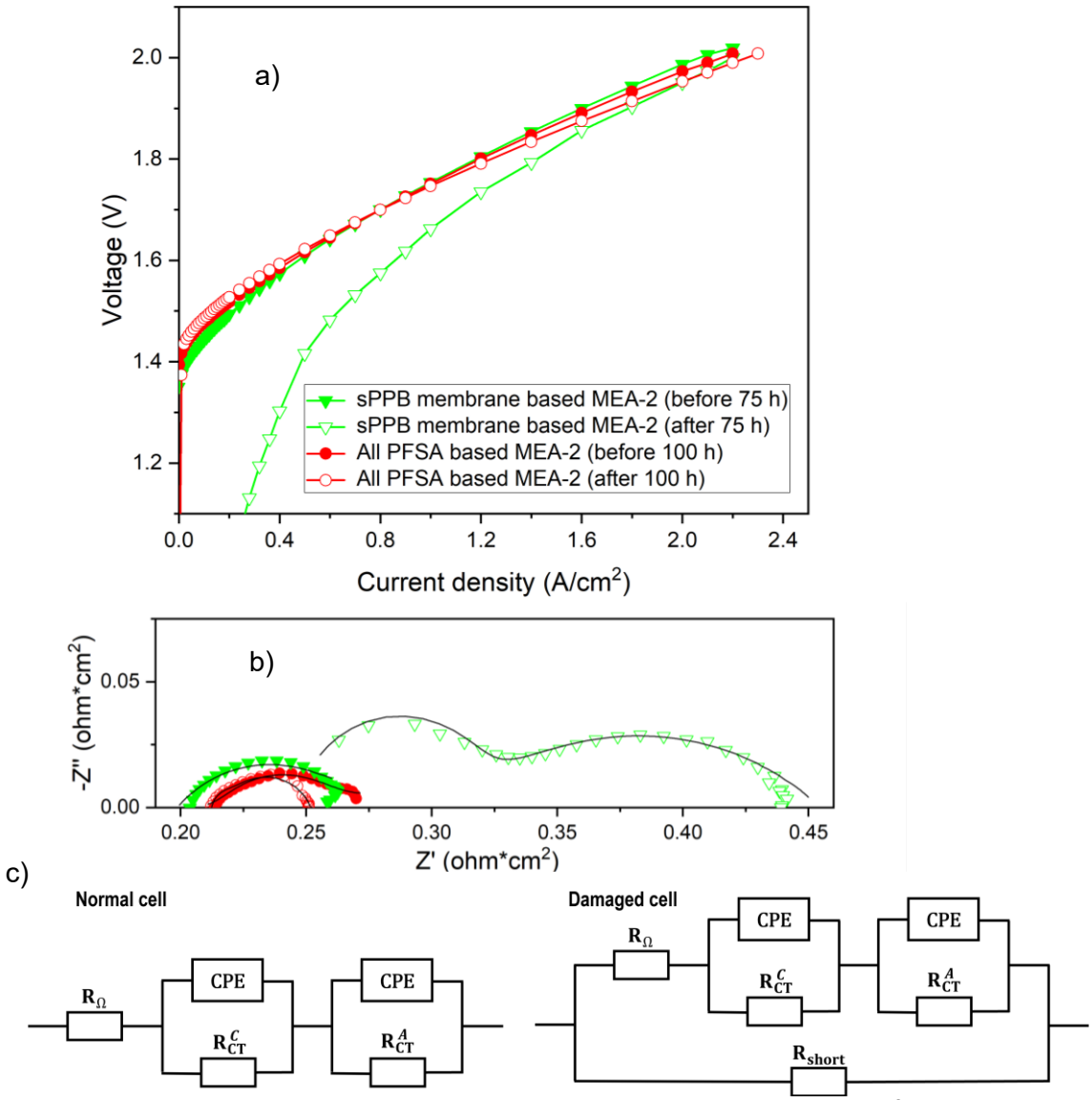

Figure 4-6 **a) Polarization curves and b) Nyquist plot (700 mA·cm^{-2}) performed at 70 °C and ambient pressure (200 mL$_{H2O}$ min^{-1}) before (solid symbols) and after (empty symbols) long time chronopotentiometry (75 h for sPPB-H^+ membrane based MEA-2 and 100 h for Nafion 112 based MEA-1). The difference between MEAs is the membrane type. C) Equivalent circuit fitting for a normal cell and a damaged cell with electrical short circuit. Adapted with permission from reference 88. Copyright 2006 Springer-Verlag.**

The soft shorting is generally related to physical damage of the membrane during fabrication of the MEA from the fibers of gas diffusion layers, the catalyst aggregates and/or the conductive impurities trapped between membrane and catalyst layers may penetrate into the membrane.[88, 89, 88] This mechanical penetration depends on the cell compression. As sPPB-H^+ is prone to excessive dimensional swelling and loss of mechanical strength soft shorting is more probable. Except for the physical damage, the chemical degradation induced pinholes can also generate soft short.

Chapter 5.

Conclusions

A non-fluorinated hydrocarbon-based PEM, made of sulfonated phenylated polyphenylene biphenyl (sPPB-H^+) was examined as an alternative to a traditional perflorosulfonic acid (PFSA) membrane, Nafion, for use in a PEMWE.

In chapter 3, sPPB-H^+ was examined as the membrane in an PEMWE cell. When measurements were performed using Nafion D520 as ionomer in the catalyst layer, sPPB-H^+ membrane (approx. 50 μm thick) provided a lower voltage of 1.70 V at 1 A cm^{-2} compared to a reference Nafion 112 membrane (1.75 V at 1 A cm^{-2}). The improvement of polarization performance is due to the much lower ohmic resistance of sPPB-H^+ membrane MEA compared to Nafion 112 MEAs. The intrinsic high proton conductivity of the sPPB-H^+ membrane is the determinant of low ohmic resistance for sPPB-H^+ membrane MEAs. The employment of sPPB-H^+ as ionomer in the catalyst layer was also investigated. The peak performance was obtained when the anodic and cathodic ionomer content were both 20 wt%. The voltage for a wholly-hydrocarbon-based sPPB-H^+ MEA was as low as 1.83 V at 1 A cm^{-2}.

In chapter 4, the stability of different MEAs in an electrolyzer cell was investigated. sPPB-H^+ membrane MEAs using Nafion D520 in the catalyst layer exhibited a higher rate of voltage increase compared to Nafion 112 MEAs. The voltage of sPPB-H^+ membrane MEAs at 1 A cm^{-2} increased, became unstable, and fell due to cell failure. The current-voltage characteristics of MEAs was analyzed using polarization curves, EIS, and gas crossover analyzed by gas chromatography. The sPPB-H^+ membrane MEA initially showed two times lower gas crossover than Nafion membranes. However, gas crossover increased over time.

Overall, the ability of sPPB-H^+ membrane to maintain its electrochemical performances over a long time in a water electrolysis cell is inferior to state-of-art PEM Nafion®. It is noted that sPPB-H^+ swells much more than Nafion and is more sensitive to the radical attack. The rate of increase in voltage at 1 A cm^{-2} is due to a loss of proton conductivity, gradual chemical degradation of the membrane, and delamination of the catalyst layer. It is speculated that oxygen gas allows the formation of peroxide radical

that attack sPPB-H^+, forms pinholes in membrane, which in turn, exacerbates gas crossover, degradation, and eventually resulting in an unstable and/or abruptly decreased voltage, and failure of the cell.

Chapter 6.

Future work

Degradation of membrane electrode assemblies during water electrolysis is complex, but mainly involves three factors: the membrane, the catalysts, and the hardware. Advancements are need in all three areas.

As the above-mentioned soft short is related to the chemical degradation induced pinholes. To figure out the degradation mechanism of the membrane, nuclear magnetic resonance, mass spectroscopy and gel permeation chromatography can be carried out to characterize the possible degradation products.[87] Hydrogen peroxide (H_2O_2) is suspected to be involved. The formation of H_2O_2 could be analyzed by using peroxidaze enzyme and UV-vis absorption spectrophotometry.[91] The ion exchange capacity of the membrane before and after the chronopotentiometry can also be measured to determine whether the degradation is preferential for the ionic group.[92] A deeper understanding of the degradation mechanism can help the future improvement of the membrane. Refer to the increasing gas crossover and related radical attack on membrane, a radical scavenger such as cerium (Ce) or manganese (Mn) ions may be explored as a route to mitigate membrane degradation.[93] To mitigate excessive swelling of polymers and reduce gas crossover, different structures of polymers may be investigated.[94] The linearity of sPPB-H^+ maybe reduced by introducing branched phenyl moieties in the backbone.[95] Compare to the sPPB-H^+ which repeating units are linked together by linear (*para*) biphenyl groups, polymers with branched moieties is considered to have lower water uptake as increased entanglement.[94,95,96]

To decrease the hydrogen crossover and reduce the probability of reaching the explosion limit of hydrogen in oxygen (3.9 vol% H_2 in O_2), PtCo alloy, which has the capacity of recombing H_2 with O_2, can be introduced between membrane and Ir as a dual-layer anodic electrode.[97] The addition of PtCo alloy electrochemically consumes permeated H_2 and also increase the electrochemical kinetics of the oxygen evolution reaction .[97]

In this thesis, the etching of flow fields was performed periodically, and the replacement of old Ti PTLs was essential. Precious metal coatings on Ti-based

components with Pt or Au can be a way to reduce the degradation of hardware.[18,98] As the high potential of anode facilitates oxidation of Ti-based components of the cell (i.e., Ti flow fields and Ti PTLs), the ohmic resistance and cell voltage will gradually increase. Pt can be deposited on Ti components to suppress oxidation and therefore simplify the daily operation (i.e., etching the flow fields from time to time and monitoring the hardware resistance every week). Future work may consider coating flow fields with Pt using thermal evaporation, sputtering, or electro-deposition. Different thickness of Pt coating affects electrical conductivity of the cell.[99]

References

(1) Bessarabov, D. *PEM Electrolysis for Hydrogen Production*; 2016. https://doi.org/10.1201/b19096.

(2) Siracusano, S.; Baglio, V.; Van Dijk, N.; Merlo, L.; Aricò, A. S. Enhanced Performance and Durability of Low Catalyst Loading PEM Water Electrolyser Based on a Short-Side Chain Perfluorosulfonic Ionomer. *Appl. Energy* **2017**, *192*, 477–489. https://doi.org/10.1016/j.apenergy.2016.09.011.

(3) Dincer, I.; Acar, C. Review and Evaluation of Hydrogen Production Methods for Better Sustainability. *Int. J. Hydrogen Energy* **2014**, *40* (34), 11094–11111. https://doi.org/10.1016/j.ijhydene.2014.12.035.

(4) Aricò, A. S.; Siracusano, S.; Briguglio, N.; Baglio, V.; Di Blasi, A.; Antonucci, V. Polymer Electrolyte Membrane Water Electrolysis: Status of Technologies and Potential Applications in Combination with Renewable Power Sources. *J. Appl. Electrochem.* **2013**, *43* (2), 107–118. https://doi.org/10.1007/s10800-012-0490-5.

(5) Ayers, K.; Danilovic, N.; Ouimet, R.; Carmo, M.; Pivovar, B.; Bornstein, M. Perspectives on Low-Temperature Electrolysis and Potential for Renewable Hydrogen at Scale. *Annu. Rev. Chem. Biomol. Eng.* **2019**, *10* (1), 219–239. https://doi.org/10.1146/annurev-chembioeng-060718-030241.

(6) Godula-Jopek; Stolten; Bourasseau. *Hydrogen Production : By Electrolysis / Edited by Agata Godula-Jopek ; with a Foreword by Detlef Stolten ; Contributors, Cyril Bourasseau [and Six Others].*; Godula-Jopek, A., Stolten, D., Bourasseau, C., Eds.; WILEY-VCH Verlag GmbH & Co. KGaA, 2015.

(7) Kim, J.; Lee, J.; Yoo, C.; Lee, K.; Lee, W. Low-Cost and Energy-Efficient Asymmetric Nickel Electrode for Alkaline Water Electrolysis. *Int. J. Hydrogen Energy* **2015**, *40* (34), 10720–10725. https://doi.org/10.1016/j.ijhydene.2015.07.025.

(8) Buttler, A.; Spliethoff, H. Current Status of Water Electrolysis for Energy Storage, Grid Balancing and Sector Coupling via Power-to-Gas and Power-to-Liquids: A Review. *Renew. Sustain. Energy Rev.* **2018**, *82* (September 2017), 2440–2454. https://doi.org/10.1016/j.rser.2017.09.003.

(9) Carmo, M.; Fritz, D. L.; Mergel, J.; Stolten, D. A Comprehensive Review on PEM Water Electrolysis. *Int. J. Hydrogen Energy* **2013**, *38* (12), 4901–4934. https://doi.org/10.1016/j.ijhydene.2013.01.151.

(10) Paidar, M.; Fateev, V.; Bouzek, K. Membrane Electrolysis—History, Current Status and Perspective. *Electrochim. Acta* **2016**, *209*, 737–756. https://doi.org/10.1016/j.electacta.2016.05.209.

(11) Siracusano, S.; Baglio, V.; Grigoriev, S. A.; Merlo, L.; Fateev, V. N. The Influence of Iridium Chemical Oxidation State on the Performance and Durability of Oxygen Evolution Catalysts in PEM Electrolysis. **2017**, *366*, 105–114. https://doi.org/10.1016/j.jpowsour.2017.09.020.

(12) Ayers, K. E.; Anderson, E. B.; Capuano, C.; Carter, B.; Dalton, L.; Hanlon, G.; Manco, J.; Niedzwiecki, M. Research Advances towards Low Cost, High Efficiency PEM Electrolysis. *ECS Trans.* **2019**, *33* (1), 3–15. https://doi.org/10.1149/1.3484496.

(13) Grigoriev, S. A.; Kalinnikov, A. A.; Millet, P.; Porembsky, V. I.; Fateev, V. N. Mathematical Modeling of High-Pressure PEM Water Electrolysis. *J. Appl. Electrochem.* **2010**, *40* (5), 921–932. https://doi.org/10.1007/s10800-009-0031-z.

(14) Chi, J.; Yu, H. Water Electrolysis Based on Renewable Energy for Hydrogen Production. *Cuihua Xuebao/Chinese J. Catal.* **2018**, *39* (3), 390–394. https://doi.org/10.1016/S1872-2067(17)62949-8.

(15) Marshall, A.; Børresen, B.; Hagen, G.; Tsypkin, M.; Tunold, R. Hydrogen Production by Advanced Proton Exchange Membrane (PEM) Water Electrolysers-Reduced Energy Consumption by Improved Electrocatalysis. *Energy* **2007**, *32* (4), 431–436. https://doi.org/10.1016/j.energy.2006.07.014.

(16) Fabbri, E.; Habereder, A.; Waltar, K.; Kötz, R.; Schmidt, T. J. Developments and Perspectives of Oxide-Based Catalysts for the Oxygen Evolution Reaction. *Catalysis Science and Technology*. Royal Society of Chemistry 2014, pp 3800–3821. https://doi.org/10.1039/c4cy00669k.

(17) Majasan, J. O.; Iacoviello, F.; Shearing, P. R.; Brett, D. J. L. Effect of Microstructure of Porous Transport Layer on Performance in Polymer Electrolyte Membrane Water Electrolyser. *Energy Procedia* **2018**, *151*, 111–119. https://doi.org/10.1016/j.egypro.2018.09.035.

(18) Shiva Kumar, S.; Himabindu, V. Hydrogen Production by PEM Water Electrolysis – A Review. *Mater. Sci. Energy Technol.* **2019**, *2* (3), 442–454. https://doi.org/10.1016/j.mset.2019.03.002.

(19) Zumdahl, S. S.; DeCoste, D. J. *Chemical Principle-8th Edition*; 2017.

(20) Kreuer, K. D. Ion Conducting Membranes for Fuel Cells and Other Electrochemical Devices. *Chemistry of Materials*. 2014, pp 361–380. https://doi.org/10.1021/cm402742u.

(21) Kumar, A. Cooperative Proton Conduction in Sulfonated and Phosphonated Hybrid Random Copolymers. *J. Mater. Chem. A* **2020**, 22632–22636. https://doi.org/10.1039/d0ta07732a.

(22) Gandini, A.; Cheradame, H. *Advances in Polymer Science.*; 1980. https://doi.org/10.1038/216619a0.

(23) Kusoglu, A.; Weber, A. Z. New Insights into Perfluorinated Sulfonic-Acid Ionomers. *Chem. Rev.* **2017**, *117* (3), 987–1104. https://doi.org/10.1021/acs.chemrev.6b00159.

(24) Zuo, Z.; Fu, Y.; Manthiram, A. A Phenomenological Theory Is Provided for Water Sorption and Proton Transport in Polymer Electrolyte Membranes (PEMs) as Well as in Polymer-Inorganic Nanocomposite Membranes (NCPEMs) That Not Only Serves to Rationalize the Sorption and Conductivity Behavi. *Polymers (Basel).* **2012**, *4* (4), 1627–1644. https://doi.org/10.3390/polym4041627.

(25) Choi, Pyoungho ; Jalani, Nikhil H ; Thampan, Tony M ; Datta, R.; Hoboken: Wiley Subscription Services, Inc., A. W. C. Consideration of Thermodynamic, Transport, and Mechanical Properties in the Design of Polymer Electrolyte Membranes for Higher Temperature Fuel Cell Operation. **2006**, *44* (1), 2183–2222. https://doi.org/10.1002/polb.

(26) Ueki, T.; Watanabe, M. Macromolecules in Ionic Liquids: Progress, Challenges, and Opportunities. *Macromolecules*. 2008, pp 3739–3749. https://doi.org/10.1021/ma800171k.

(27) Sata, T. *Ion Exchange Membranes: Preparation, Characterization, Modification and Application*; Royal Society of Chemistry: Tokuyama City, 2004.

(28) Kundu, P. P.; Dutta, K. *Progress and Recent Trends in Microbial Fuel Cells*; Elsevier, 2018.

(29) O' Hayre, R. P.; Cha, S.-W.; Colella, W. G.; Prinz, F. B. *Fuel Cell Fundamentals, 3rd Edition*; John Wiley & Sons, 2016.

(30) Soboleva, T.; Xie, Z.; Shi, Z.; Tsang, E.; Navessin, T.; Holdcroft, S. Investigation of the Through-Plane Impedance Technique for Evaluation of Anisotropy of Proton Conducting Polymer Membranes. *J. Electroanal. Chem.* **2008**, *622* (2), 145–152. https://doi.org/10.1016/j.jelechem.2008.05.017.

(31) Yang, S.-Y. *Advanced Polyimide Materials : Synthesis, Characterization, and Applications*; Elsevier, 2018. https://doi.org/10.1016/B978-0-12-812640-0.00007-X.

(32) Ito, H.; Maeda, T.; Nakano, A.; Takenaka, H. Properties of Nafion Membranes under PEM Water Electrolysis Conditions. *International Journal of Hydrogen Energy*. Elsevier Ltd 2011, pp 10527–10540. https://doi.org/10.1016/j.ijhydene.2011.05.127.

(33) Grigoriev, S. A.; Porembskiy, V. I.; Korobtsev, S. V.; Fateev, V. N.; Auprêtre, F.; Millet, P. High-Pressure PEM Water Electrolysis and Corresponding Safety Issues. *Int. J. Hydrogen Energy* **2011**, *36* (3), 2721–2728. https://doi.org/10.1016/j.ijhydene.2010.03.058.

(34) Schalenbach, M.; Carmo, M.; Fritz, D. L.; Mergel, J.; Stolten, D. Pressurized PEM

Water Electrolysis: Efficiency and Gas Crossover. *Int. J. Hydrogen Energy* **2013**, *38* (35), 14921–14933. https://doi.org/10.1016/j.ijhydene.2013.09.013.

(35) Grigoriev, S. A.; Millet, P.; Korobtsev, S. V.; Porembskiy, V. I.; Pepic, M.; Etievant, C.; Puyenchet, C.; Fateev, V. N. Hydrogen Safety Aspects Related to High-Pressure Polymer Electrolyte Membrane Water Electrolysis. *Int. J. Hydrogen Energy* **2009**, *34* (14), 5986–5991. https://doi.org/10.1016/j.ijhydene.2009.01.047.

(36) Carmo, M.; Fritz, D. L.; Mergel, J.; Stolten, D. A Comprehensive Review on PEM Water Electrolysis. *Int. J. Hydrogen Energy* **2013**, *38* (12), 4901–4934. https://doi.org/10.1016/j.ijhydene.2013.01.151.

(37) Holdcroft, S. Fuel Cell Catalyst Layers: A Polymer Science Perspective. *Chem. Mater.* **2014**, *26* (1), 381–393. https://doi.org/10.1021/cm401445h.

(38) Lee, J.; Ahn, Y.; Kim, D. Binder Effect on Fuel Cell Performance and Interfacial Stability of Membrane Electrode Assembly Fabricated with Sulfonated Poly(Ether Ether Ketone) Membrane. *Macromol. Res.* **2019**, *27* (2), 175–181. https://doi.org/10.1007/s13233-019-7063-y.

(39) McGovern, M. S.; Garnett, E. C.; Rice, C.; Masel, R. I.; Wieckowski, A. Effects of Nafion as a Binding Agent for Unsupported Nanoparticle Catalysts. *J. Power Sources* **2003**, *115* (1), 35–39. https://doi.org/10.1016/S0378-7753(02)00623-7.

(40) Lee, M.; Uchida, M.; Yano, H.; Tryk, D. A.; Uchida, H.; Watanabe, M. New Evaluation Method for the Effectiveness of Platinum/Carbon Electrocatalysts under Operating Conditions. *Electrochim. Acta* **2010**, *55* (28), 8504–8512. https://doi.org/10.1016/j.electacta.2010.07.071.

(41) Vincent, I.; Bessarabov, D. Low Cost Hydrogen Production by Anion Exchange Membrane Electrolysis: A Review. *Renew. Sustain. Energy Rev.* **2018**, *81* (August 2016), 1690–1704. https://doi.org/10.1016/j.rser.2017.05.258.

(42) Mauritz, K. A.; Moore, R. B. State of Understanding of Nafion. **2004**. https://doi.org/10.1021/cr0207123.

(43) Tsuchiya, H.; Kobayashi, O. Mass Production Cost of PEM Fuel Cell by Learning Curve. *Int. J. Hydrogen Energy* **2004**, *29* (10), 985–990. https://doi.org/10.1016/j.ijhydene.2003.10.011.

(44) Kreuer, K. D. On the Development of Proton Conducting Polymer Membranes for Hydrogen and Methanol Fuel Cells. **2001**, *185*, 29–39.

(45) Smitha, B.; Sridhar, S.; Khan, A. A. Solid Polymer Electrolyte Membranes for Fuel Cell Applications - A Review. *J. Memb. Sci.* **2005**, *259* (1–2), 10–26. https://doi.org/10.1016/j.memsci.2005.01.035.

(46) Wei, G.; Xu, L.; Huang, C.; Wang, Y. SPE Water Electrolysis with SPEEK/PES

Blend Membrane. *Int. J. Hydrogen Energy* **2010**, *35* (15), 7778–7783. https://doi.org/10.1016/j.ijhydene.2010.05.041.

(47) Masson, J. P.; Molina, R.; Roth, E.; Gaussens, G.; Lemaire, F. Obtention and Evaluation of Polyethylene-Based Solid Polymer Electrolyte Membranes for Hydrogen Production. *Int. J. Hydrogen Energy* **1982**, *7* (2), 167–171. https://doi.org/10.1016/0360-3199(82)90143-4.

(48) Linkous, C.; Slattery, D. Water Electrolysis at Elevated Temperature Using Ionomer Membranes. 1993, p 7.

(49) Linkous, C.; Slattery, D.; Kopitzke, R.; Muradov, N. Contact Report:Sustainable Hydrogen Production. Floride Solar Energy 1999, p 153.

(50) Linkous, C. A.; Anderson, H. R.; Kopitzke, R. W.; Nelson, G. L. Development of New Proton Exchange Membrane Electrolytes for Water Electrolysis at Higher Temperatures. *Int. J. Hydrogen Energy* **1998**, *23* (7), 525–529. https://doi.org/10.1016/s0360-3199(97)00113-4.

(51) Bystron, T.; Vesely, M.; Paidar, M.; Papakonstantinou, G.; Sundmacher, K.; Bensmann, B.; Hanke-Rauschenbach, R.; Bouzek, K. Enhancing PEM Water Electrolysis Efficiency by Reducing the Extent of Ti Gas Diffusion Layer Passivation. *J. Appl. Electrochem.* **2018**, *48* (6), 713–723. https://doi.org/10.1007/s10800-018-1174-6.

(52) Marshall, A. T.; Sunde, S.; Tsypkin, M.; Tunold, R. Performance of a PEM Water Electrolysis Cell Using Irx Ruy Taz O2 Electrocatalysts for the Oxygen Evolution Electrode. *Int. J. Hydrogen Energy* **2007**, *32* (13), 2320–2324. https://doi.org/10.1016/j.ijhydene.2007.02.013.

(53) Klose, C.; Saatkamp, T.; Münchinger, A.; Bohn, L.; Titvinidze, G.; Breitwieser, M.; Kreuer, K. D.; Vierrath, S. All-Hydrocarbon MEA for PEM Water Electrolysis Combining Low Hydrogen Crossover and High Efficiency. *Adv. Energy Mater.* **2020**, *10* (14), 1–9. https://doi.org/10.1002/aenm.201903995.

(54) Kumar, S. S.; Himabindu, V. Hydrogen Production by PEM Water Electrolysis – A Review. *Mater. Sci. Energy Technol.* **2019**, *2* (3), 442–454. https://doi.org/10.1016/j.mset.2019.03.002.

(55) Schmidt, O.; Gambhir, A.; Staffell, I.; Hawkes, A.; Nelson, J.; Few, S. Future Cost and Performance of Water Electrolysis: An Expert Elicitation Study. *Int. J. Hydrogen Energy* **2017**, *42* (52), 30470–30492. https://doi.org/10.1016/j.ijhydene.2017.10.045.

(56) Sun, X.; Xu, K.; Fleischer, C.; Liu, X.; Grandcolas, M.; Strandbakke, R.; Bjørheim, T. S.; Norby, T.; Chatzitakis, A. Earth-Abundant Electrocatalysts in Proton Exchange Membrane Electrolyzers. *Catalysts* **2018**, *8* (12). https://doi.org/10.3390/catal8120657.

(57) Jang, I. Y.; Kweon, O. H.; Kim, K. E.; Hwang, G. J.; Moon, S. B.; Kang, A. S. Application of Polysulfone (PSf)- and Polyether Ether Ketone (PEEK)-Tungstophosphoric Acid (TPA) Composite Membranes for Water Electrolysis. *J. Memb. Sci.* **2008**, *322* (1), 154–161. https://doi.org/10.1016/j.memsci.2008.05.028.

(58) Siracusano, S.; Baglio, V.; Lufrano, F.; Staiti, P.; Aricò, A. S. Electrochemical Characterization of a PEM Water Electrolyzer Based on a Sulfonated Polysulfone Membrane. *J. Memb. Sci.* **2013**, *448*, 209–214. https://doi.org/10.1016/j.memsci.2013.07.058.

(59) Skulimowska, A.; Dupont, M.; Zaton, M.; Sunde, S.; Merlo, L.; Jones, D. J.; Rozière, J. Proton Exchange Membrane Water Electrolysis with Short-Side-Chain Aquivion® Membrane and IrO2 Anode Catalyst. *Int. J. Hydrogen Energy* **2014**, *39* (12), 6307–6316. https://doi.org/10.1016/j.ijhydene.2014.02.082.

(60) Adamski, M.; Skalski, T. J. G.; Britton, B.; Peckham, T. J.; Metzler, L.; Holdcroft, S. Highly Stable, Low Gas Crossover, Proton-Conducting Phenylated Polyphenylenes. *Angew. Chemie - Int. Ed.* **2017**, *56* (31), 9058–9061. https://doi.org/10.1002/anie.201703916.

(61) Nolte, R.; Ledjeff, K.; Bauer, M.; Mülhaupt, R. Partially Sulfonated Poly(Arylene Ether Sulfone) - A Versatile Proton Conducting Membrane Material for Modern Energy Conversion Technologies. *J. Memb. Sci.* **1993**, *83* (2), 211–220. https://doi.org/10.1016/0376-7388(93)85268-2.

(62) Berresheim, A. J.; Müller, M.; Müllen, K. Polyphenylene Nanostructures. *Chem. Rev.* **1999**, *99* (7), 1747–1785. https://doi.org/10.1021/cr970073+.

(63) Granados-Focil, S.; Litt, M. H. A New Class of Polyelectrolytes, Polyphenylene Sulfonic Acids and Its Copolymers, as Proton Exchange Membranes for PEMFC's. *ACS Natl. Meet. B. Abstr.* **2004**, *228* (1).

(64) Fujimoto, C. H.; Hickner, M. A.; Cornelius, C. J.; Loy, D. A. Ionomeric Poly(Phenylene) Prepared by Diels-Alder Polymerization: Synthesis and Physical Properties of a Novel Polyelectrolyte. *Macromolecules* **2005**, *38* (12), 5010–5016. https://doi.org/10.1021/ma0482720.

(65) Wu, S.; Qiu, Z.; Zhang, S.; Yang, X.; Yang, F.; Li, Z. The Direct Synthesis of Wholly Aromatic Poly(p-Phenylene)s Bearing Sulfobenzoyl Side Groups as Proton Exchange Membranes. *Polymer (Guildf).* **2006**, *47* (20), 6993–7000. https://doi.org/10.1016/j.polymer.2006.08.017.

(66) Goto, K.; Rozhansk, I.; Yamakawa, Y.; Otsuki, T.; Naito, Y. Development of Aromatic Polymer Electrolyte Membrane with High Conductivity and Durability for Fuel Cell. *Polym. J.* **2009**, *41* (2), 95–104. https://doi.org/10.1295/polymj.PJ2008220.

(67) Skalski, T. J. G.; Britton, B.; Peckham, T. J.; Holdcroft, S. Structurally-Defined,

Sulfo-Phenylated, Oligophenylenes and Polyphenylenes. *J. Am. Chem. Soc.* **2015**, *137* (38), 12223–12226. https://doi.org/10.1021/jacs.5b07865.

(68) Ojong, E. T.; Kwan, J. T. H.; Nouri-Khorasani, A.; Bonakdarpour, A.; Wilkinson, D. P.; Smolinka, T. Development of an Experimentally Validated Semi-Empirical Fully-Coupled Performance Model of a PEM Electrolysis Cell with a 3-D Structured Porous Transport Layer. *Int. J. Hydrogen Energy* **2017**, *42* (41), 25831–25847. https://doi.org/10.1016/j.ijhydene.2017.08.183.

(69) Seo, S. J.; Woo, J. J.; Yun, S. H.; Lee, H. J.; Park, J. S.; Xu, T.; Yang, T. H.; Lee, J.; Moon, S. H. Analyses of Interfacial Resistances in a Membrane-Electrode Assembly for a Proton Exchange Membrane Fuel Cell Using Symmetrical Impedance Spectroscopy. *Phys. Chem. Chem. Phys.* **2010**, *12* (46), 15291–15300. https://doi.org/10.1039/c0cp00662a.

(70) Bagotsky, V. S. *Fundamentals of Electrochemistry*; John Wiley & Sons, Inc., 2006; Vol. 5.

(71) Barsoukov, E.; Macdonald, J. R. *Impedance Spectroscopy: Theory,Experimen, and Applications*; John Wiley & Sons, 2005. https://doi.org/10.1002/0471716243.ch3.

(72) Siracusano, S.; Trocino, S.; Briguglio, N.; Baglio, V.; Aricò, A. S. Electrochemical Impedance Spectroscopy as a Diagnostic Tool in Polymer Electrolyte Membrane Electrolysis. *Materials (Basel).* **2018**, *11* (8). https://doi.org/10.3390/ma11081368.

(73) Bard, A. J.; Faulkner, L. R. *Electrochemical Methods: Fundamentals and Applications*, 2nd ed.; New York, 2001. https://doi.org/10.1038/s41929-019-0277-8.

(74) Yuan, X.-Z. Y.; Song, C.; Wang, H.; Zhang, J. *Electrochemical Impedance Spectroscopy in PEM Fuel Cells:Fundamentals and Applications*; Springer, 2009.

(75) Frensch, S. H.; Olesen, A. C.; Araya, S. S.; Kær, S. K. Model-Supported Characterization of a PEM Water Electrolysis Cell for the Effect of Compression. *Electrochim. Acta* **2018**, *263* (February), 228–236. https://doi.org/10.1016/j.electacta.2018.01.040.

(76) Orazem, M. E.; Pébère, N.; Tribollet, B. Enhanced Graphical Representation of Electrochemical Impedance Data. *J. Electrochem. Soc.* **2006**, *153* (4), B129. https://doi.org/10.1149/1.2168377.

(77) Bessarabov, D.; Kruger, A.; Luopa, S. M.; Park, J.; Molnar, A. A.; Lewinski, K. A. Gas Crossover Mitigation in PEM Water Electrolysis: Hydrogen Cross-over Benchmark Study of 3M's Ir-NSTF Based Electrolysis Catalyst-Coated Membranes. *ECS Trans.* **2016**, *75* (14), 1165–1173. https://doi.org/10.1149/07514.1165ecst.

(78) Lee, C. H.; Park, H. B.; Lee, Y. M.; Lee, R. D. Importance of Proton Conductivity

Measurement in Polymer Electrolyte Membrane for Fuel Cell Application. *Ind. Eng. Chem. Res.* **2005**, *44* (20), 7617–7626. https://doi.org/10.1021/ie0501172.

(79) Arblaster, J. W. Selected Electrical Resistivity Values for the Platinum Group of Metals Part III: Ruthenium and Osmium: Improved Values Obtained for Ruthenium and Osmium. *Johnson Matthey Technol. Rev.* **2016**, *60* (3), 179–185. https://doi.org/10.1595/205651316X691618.

(80) Peron, J.; Mani, A.; Zhao, X.; Edwards, D.; Adachi, M.; Soboleva, T.; Shi, Z.; Xie, Z.; Navessin, T.; Holdcroft, S. Properties of Nafion® NR-211 Membranes for PEMFCs. *J. Memb. Sci.* **2010**, *356* (1–2), 44–51. https://doi.org/10.1016/j.memsci.2010.03.025.

(81) Cho, M. K.; Park, H. Y.; Lee, H. J.; Kim, H. J.; Lim, A.; Henkensmeier, D.; Yoo, S. J.; Kim, J. Y.; Lee, S. Y.; Park, H. S.; Jang, J. H. Alkaline Anion Exchange Membrane Water Electrolysis: Effects of Electrolyte Feed Method and Electrode Binder Content. *J. Power Sources* **2018**, *382* (November 2017), 22–29. https://doi.org/10.1016/j.jpowsour.2018.02.025.

(82) Malevich, D.; Halliop, E.; Peppley, B. A.; Pharoah, J. G.; Karan, K. Investigation of Charge-Transfer and Mass-Transport Resistances in PEMFCs with Microporous Layer Using Electrochemical Impedance Spectroscopy. *J. Electrochem. Soc.* **2009**, *156* (2), B216. https://doi.org/10.1149/1.3033408.

(83) Lettenmeier, P.; Wang, R.; Abouatallah, R.; Helmly, S.; Morawietz, T.; Hiesgen, R.; Kolb, S.; Burggraf, F.; Kallo, J.; Gago, A. S.; Friedrich, K. A. Durable Membrane Electrode Assemblies for Proton Exchange Membrane Electrolyzer Systems Operating at High Current Densities. *Electrochim. Acta* **2016**, *210*, 502–511. https://doi.org/10.1016/j.electacta.2016.04.164.

(84) Rasten, E.; Hagen, G.; Tunold, R. Electrocatalysis in Water Electrolysis with Solid Polymer Electrolyte. *Electrochim. Acta* **2003**, *48* (25–26), 3945–3952. https://doi.org/10.1016/j.electacta.2003.04.001.

(85) Rozain, C.; Mayousse, E.; Guillet, N.; Millet, P. Influence of Iridium Oxide Loadings on the Performance of PEM Water Electrolysis Cells: Part II - Advanced Oxygen Electrodes. *Appl. Catal. B Environ.* **2016**, *182*, 123–131. https://doi.org/10.1016/j.apcatb.2015.09.011.

(86) Chandesris, M.; Médeau, V.; Guillet, N.; Chelghoum, S.; Thoby, D.; Fouda-Onana, F. Membrane Degradation in PEM Water Electrolyzer: Numerical Modeling and Experimental Evidence of the Influence of Temperature and Current Density. *Int. J. Hydrogen Energy* **2015**, *40* (3), 1353–1366. https://doi.org/10.1016/j.ijhydene.2014.11.111.

(87) Holmes, T.; Skalski, T. J. G.; Adamski, M.; Holdcroft, S. Stability of Hydrocarbon Fuel Cell Membranes: Reaction of Hydroxyl Radicals with Sulfonated Phenylated Polyphenylenes. *Chem. Mater.* **2019**, *31* (4), 1441–1449. https://doi.org/10.1021/acs.chemmater.8b05302.

(88) Badwal, S. P. S.; Giddey, S.; Ciacchi, F. T. Hydrogen and Oxygen Generation with Polymer Electrolyte Membrane (PEM)-Based Electrolytic Technology. *Ionics (Kiel).* **2006**, *12* (1), 7–14. https://doi.org/10.1007/s11581-006-0002-x.

(89) Gittleman, C. S.; Coms, F. D.; Lai, Y. H. *Membrane Durability: Physical and Chemical Degradation*; Elsevier Inc., 2011. https://doi.org/10.1016/B978-0-12-386936-4.10002-8.

(90) Weber, A. Z. Gas-Crossover and Membrane-Pinhole Effects in Polymer-Electrolyte Fuel Cells. *J. Electrochem. Soc.* **2008**, *155* (6), B521. https://doi.org/10.1149/1.2898130.

(91) Inaba, M.; Kinumoto, T.; Kiriake, M.; Umebayashi, R.; Tasaka, A.; Ogumi, Z. Gas Crossover and Membrane Degradation in Polymer Electrolyte Fuel Cells. *Electrochim. Acta* **2006**, *51* (26), 5746–5753. https://doi.org/10.1016/j.electacta.2006.03.008.

(92) Stucki, S.; Scherer, G. G.; Schlagowski, S.; Fischer, E. PEM Water Electrolysers: Evidence for Membrane Failure in 100 KW Demonstration Plants. *J. Appl. Electrochem.* **1998**, *28* (10), 1041–1049. https://doi.org/10.1023/A:1003477305336.

(93) Gubler, L.; Koppenol, W. H. Kinetic Simulation of the Chemical Stabilization Mechanism in Fuel Cell Membranes Using Cerium and Manganese Redox Couples. *J. Electrochem. Soc.* **2011**, *159* (2), B211–B218. https://doi.org/10.1149/2.075202jes.

(94) Peressin, N.; Adamski, M.; Holdcroft, S. Effect of Steric Constraints on the Physico-Electrochemical Properties of Sulfonated Polyaromatic Copolymers. *Polym. Int.* **2021**, *70* (1), 96–106. https://doi.org/10.1002/pi.6097.

(95) Rodgers, M.; Yang, Y.; Holdcroft, S. A Study of Linear versus Angled Rigid Rod Polymers for Proton Conducting Membranes Using Sulfonated Polyimides. *Eur. Polym. J.* **2006**, *42* (5), 1075–1085. https://doi.org/10.1016/j.eurpolymj.2005.11.011.

(96) Peressin, N.; Adamski, M.; Schibli, E. M.; Ye, E.; Frisken, B. J.; Holdcroft, S. Structure-Property Relationships in Sterically Congested Proton-Conducting Poly(Phenylene)s: The Impact of Biphenyl Linearity. *Macromolecules* **2020**. https://doi.org/10.1021/acs.macromol.0c00310.

(97) Briguglio, N.; Siracusano, S.; Bonura, G.; Sebastián, D.; Aricò, A. S. Flammability Reduction in a Pressurised Water Electrolyser Based on a Thin Polymer Electrolyte Membrane through a Pt-Alloy Catalytic Approach. *Appl. Catal. B Environ.* **2019**, *246* (October 2018), 254–265. https://doi.org/10.1016/j.apcatb.2018.12.079.

(98) Feng, Q.; Yuan, X. Z.; Liu, G.; Wei, B.; Zhang, Z.; Li, H.; Wang, H. A Review of Proton Exchange Membrane Water Electrolysis on Degradation Mechanisms and

Mitigation Strategies. *J. Power Sources* **2017**, *366*, 33–55. https://doi.org/10.1016/j.jpowsour.2017.09.006.

(99) Jung, H. Y.; Huang, S. Y.; Popov, B. N. High-Durability Titanium Bipolar Plate Modified by Electrochemical Deposition of Platinum for Unitized Regenerative Fuel Cell (URFC). *J. Power Sources* **2010**, *195* (7), 1950–1956. https://doi.org/10.1016/j.jpowsour.2009.10.002.

Appendix A. An example of Agilent GC report

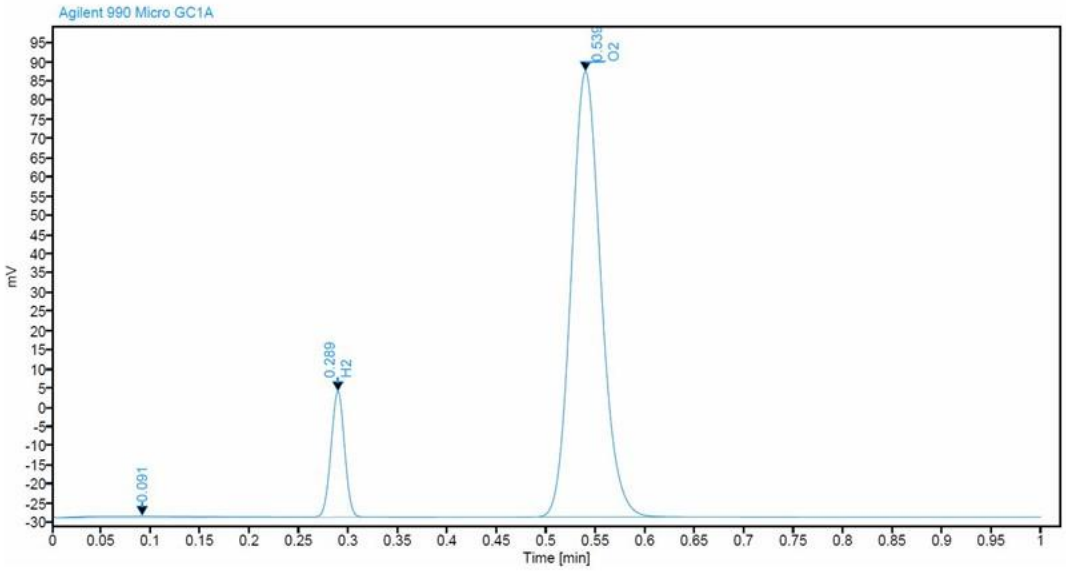

Name	RT (min)	Area	RF	Calib Amount []	Amount	Concentration
H2	0.289	31.441	26.351		1.193	1.1932
O2	0.539	242.021	2.479		97.617	97.6165
	Sum	273.4618			98.810	98.8097

Figure A1. Gas chromatogram output from Agilent 990 Micro GC showing the separation of anodic gas.

Compound: **H2**

Signal: Agilent 990 Micro GC1A

Exp. RT: 0.289

Residual: 9.22690

R: 0.99688

R^2: 0.99376

Formula: y = ax + b

a: 21.5909

b: 5.6794

c:

d:

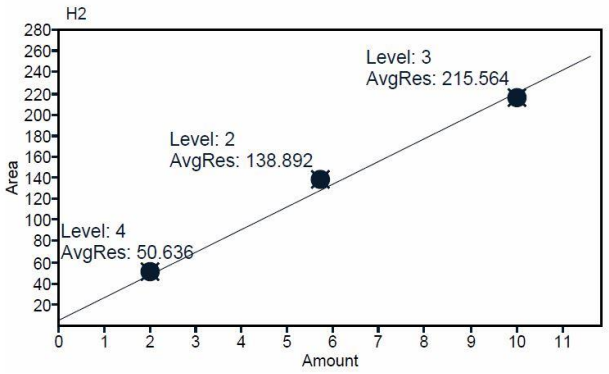

Compound: **O2**

Signal: Agilent 990 Micro GC1A

Exp. RT: 0.540

Residual:

R: 1.00000

R^2: 1.00000

Formula: y = ax + b

a: 2.4793

b: 0.0000

c:

d:

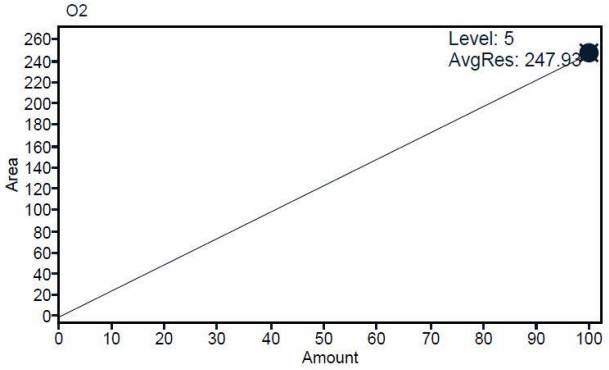

Figure A2. Calibration of H_2 in the mixture gas using 2, 5.71 and 10 vol% H_2 in N_2 standard gas. Calibration of O_2 using 99.998 % O_2.

Appendix B. Etching of Ti flow fields

Ti is the most commonly used material for bipolar plates and PTLs of PEMWEs. However, Ti shows gradual oxidation under ambient conditions, especially for anode compartment of water electrolysis where anode is polarized to a high potential. The presence of semi-/nonconducting oxide layer has a negative effect on the electrolysis performance: an increase in contact resistance, however, it also prevents the Ti from further oxidation due to high stability.[1,2,3] The oxidation of Ti materials (i.e., Ti flow fields and Ti PTLs) is inevitable during water electrolysis and so the dry hardware resistance is measured every week using potentiostatic electrochemical impedance spectroscopy (EIS) at 0 V with the AC perturbation at 10 mV. When the hardware resistance is over 50 mΩ cm^2, new Ti PTLs are used. When the hardware resistance is over 75 mΩ cm^2 and exchange the new Ti PTLs does not improve the condition, the etching of the flow fields is performed.

The etching was performed by immersing Ti flow fields in an oxalic acid solution (15%) at 77 °C for 45 min and then in concentrated sulfuric acid (96%) for 2 s. After chemical etching, Ti was washed several times in hot DI water. The impurities and passivation layer were removed after etching (**Table B1**). The hardware impedance was decreased (**Table B2**).

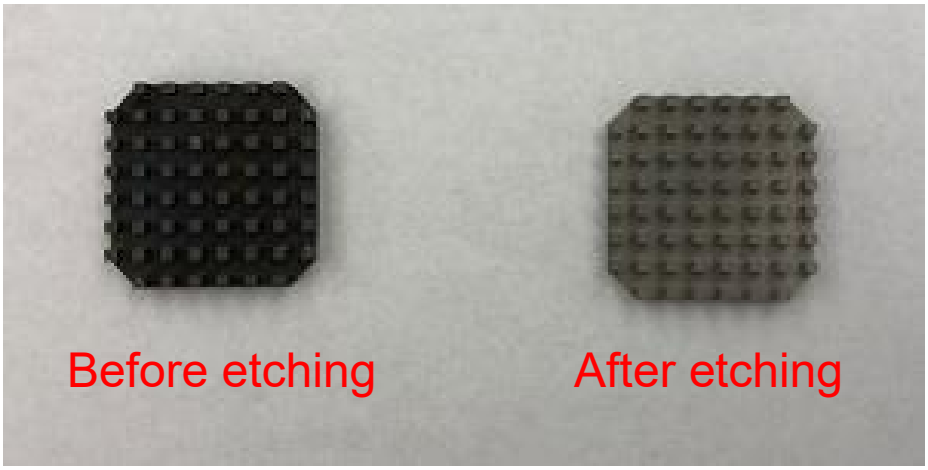

Table B1 Apperance of Ti flow field before and after etching

Table B2 Mass of flow fields change and hardware resistance change before and after etching

	Before etching	After etching
Weight of anodic flow field (g)	3.8947	3.8543
Weight of cathodic flow field (g)	3.9067	3.8833
Hardware resistances (mΩ cm^2)	81.5	21.5

(1) Bystron, T.; Vesely, M.; Paidar, M.; Papakonstantinou, G.; Sundmacher, K.; Bensmann, B.; Hanke-Rauschenbach, R.; Bouzek, K. Enhancing PEM Water Electrolysis Efficiency by Reducing the Extent of Ti Gas Diffusion Layer Passivation. *J. Appl. Electrochem.* **2018**, *48* (6), 713–723. https://doi.org/10.1007/s10800-018-1174-6.

(2) Jung, H. Y.; Huang, S. Y.; Popov, B. N. High-Durability Titanium Bipolar Plate Modified by Electrochemical Deposition of Platinum for Unitized Regenerative Fuel Cell (URFC). *J. Power Sources* **2010**, *195* (7), 1950–1956. https://doi.org/10.1016/j.jpowsour.2009.10.002.

(3) Iniesta, J.; González-García, J.; Fernández, J.; Montiel, V.; Aldaz, A. On the Voltammetric Behavior of a Platinized Titanium Surface with Respect to the Specific Hydrogen and Anion Adsorption and Charge Transfer Processes. *J. Mater. Chem.* **1999**, *9* (12), 3141–3145. https://doi.org/10.1039/a903479j.

Appendix C. Conductivity of circulation water and photos of electrodes and MEAs

18.2 MΩ deionized water was fed through the Greenlight electrolyzer test station (ETS) to anode and cathode compartments of the cell and re-circulated at 200 mL min^{-1}. The initial conductivity for the 18.2 MΩ deionized water is around 0.4 to 0.5 μS cm^{-1}. The conductivity of the water was also tested after water electrolysis measurements (i.e., polarization curves, electrochemical impedance spectroscopy and chronopotentiometry).

Table C1 Conductivity of circulation water before and after chronopotentiometry for all PFSA based MEA (upper), for sPPB-H^+ membrane based MEA (middle) and for wholly-sPPB-H^+ based MEA. (bottom).

All PFSA based MEAs	Cathodic circulation water (μS cm^{-1})	Anodic circulation water (μS cm^{-1})
Before WE test	0.56	0.60
After WE test (with 100-h chronopotentiometry)	0.62	0.76

sPPB-H^+ membrane based MEA	Cathodic circulation water (μS cm^{-1})	Anodic circulation water (μS cm^{-1})
Before WE test	0.40	0.44
After WE test (with 100-h chronopotentiometry)	0.65	1.27

Wholly-sPPB-H^+ based MEA	Cathodic circulation water (μS cm^{-1})	Anodic circulation water (μS cm^{-1})
Before WE test	0.44	0.43
After WE test (no chronopotentiometry)	0.64	1.19
After WE test (with 5-h chronopotentiometry)	1.07	7.25

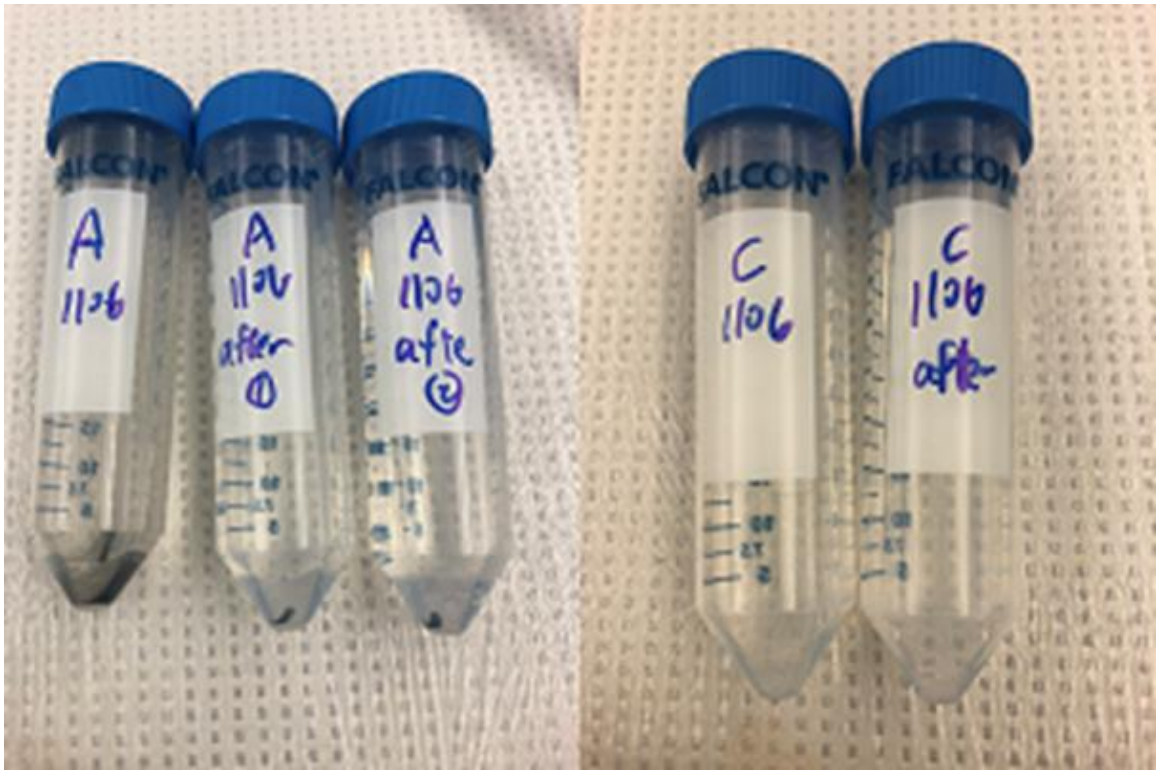

Figure C1 **Photographs of circulation water collected from the ETS anodic and cathodic reservoir after chronopotentiometry for wholly-hydrocarbon based MEAs using sPPB-H^+ as membrane and in the catalyst, after one time exchange of fresh 18.2 MΩ deionized water (after ①) and after second time exchange of reservoir water (after ②).**

.

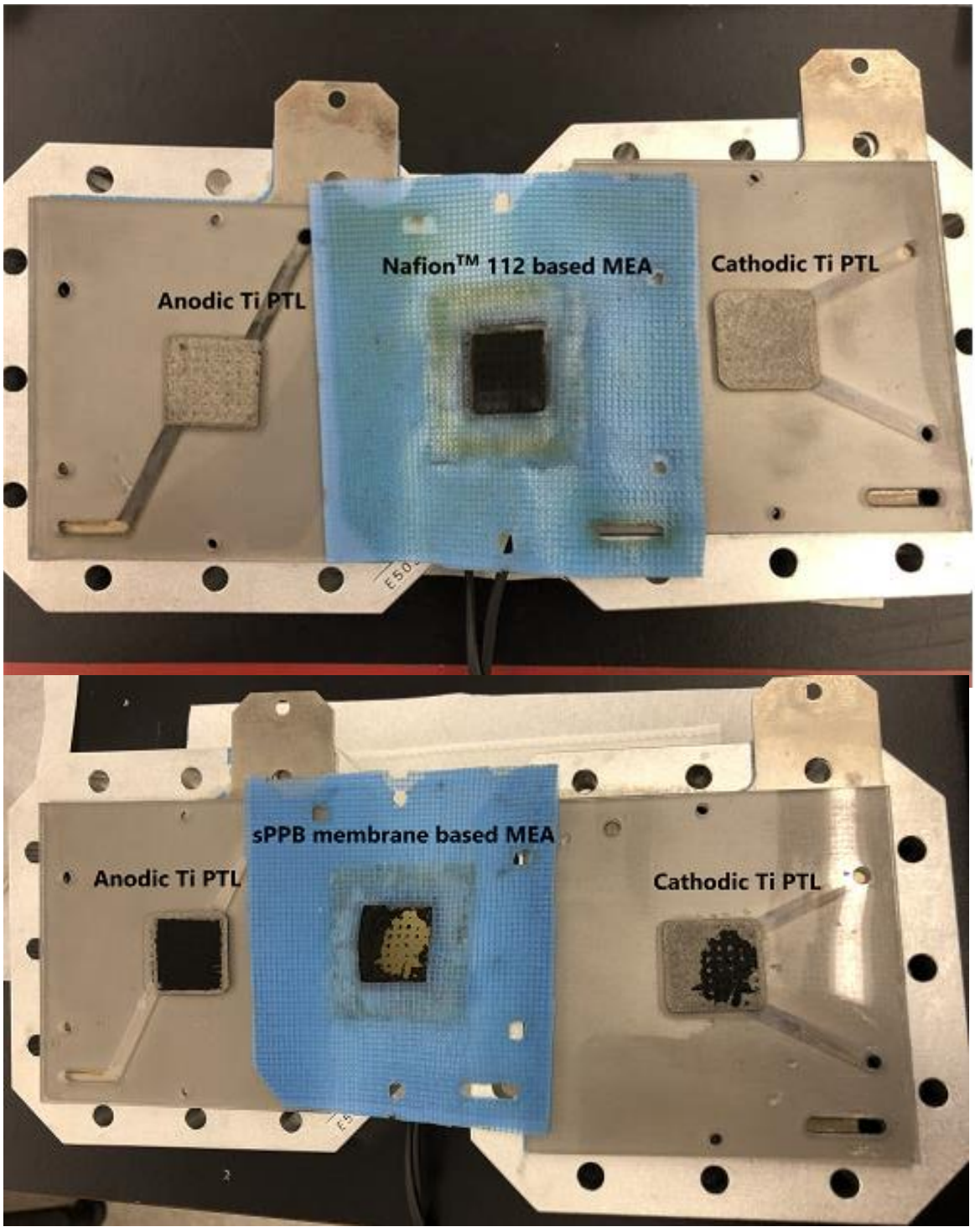

Figure C2 **Photographs of anodic PTL, cathodic PTLs and MEAs after electrochemical tests (without chronopotentiometry) for wholly PFSA based MEA (upper) and for sPPB-H^+ membrane based MEA (bottom).**

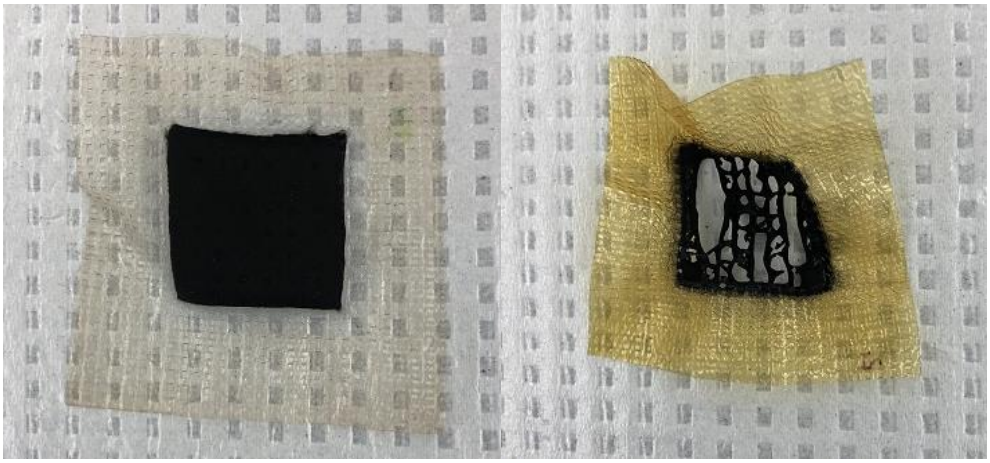

Figure C3 **Photographs of Nafion 112 based MEA and sPPB-H^+ membrane based MEA after long term duraibility test (70 °C, 200 mL_{H_2O} min^{-1}). These MEAs contain ~3.5 mg_{Ir} cm^{-2}, 10 wt% Nafion® ionomer in anode and ~1.0 mg_{Pt} cm^{-2} 20 wt% Nafion® ionomer in cathode. The difference between MEAs is the membrane type.**

Appendix D. Scanning electron microscopy (SEM) images of membrane-electrode assemblies (MEAs)

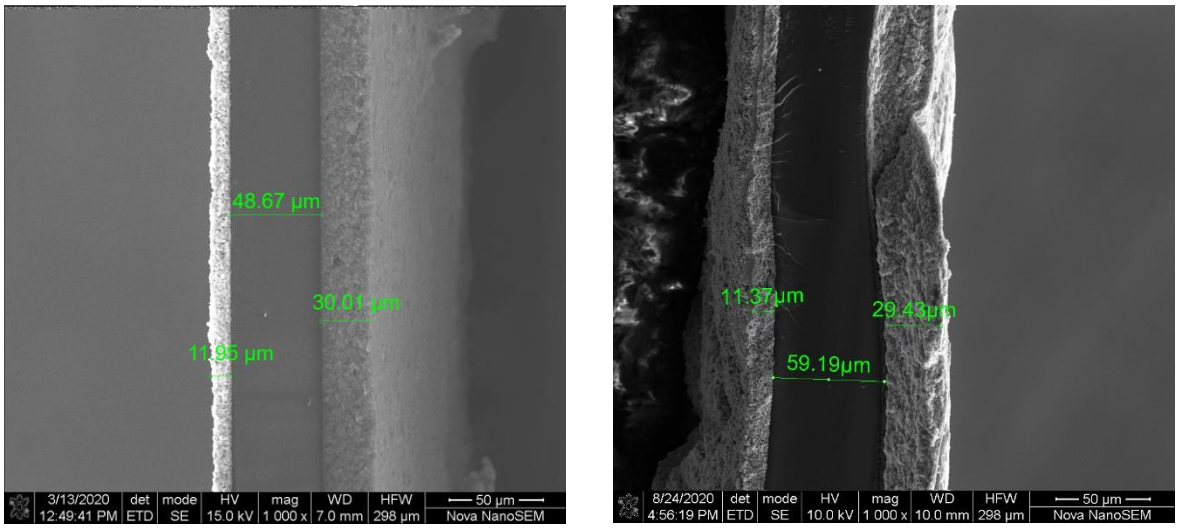

Figure D1 **Cross-section unused (left) and used (right) Nafion 112 membrane based dry MEAs using Scanning Electron Microscopy (SEM). The MEA contains ~3.5 mg_{Ir} cm^{-2}, 10 wt% Nafion® ionomer in anode and ~1.0 mg_{Pt} cm^{-2} 20 wt% Nafion® ionomer in cathode.**

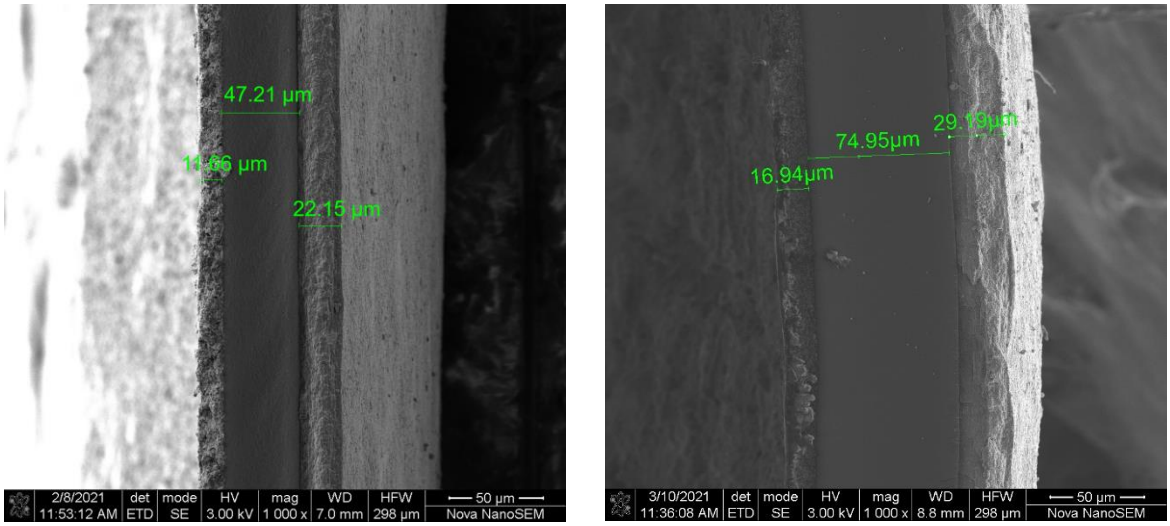

Figure D2 **Cross-section unused (left) and used (right) sPPB-H^+ membrane based dry MEAs using Scanning Electron Microscopy (SEM). The MEA contains ~3.5 mg_{Ir} cm^{-2}, 10 wt% Nafion® ionomer in anode and ~1.0 mg_{Pt} cm^{-2} 20 wt% Nafion® ionomer in cathode.**

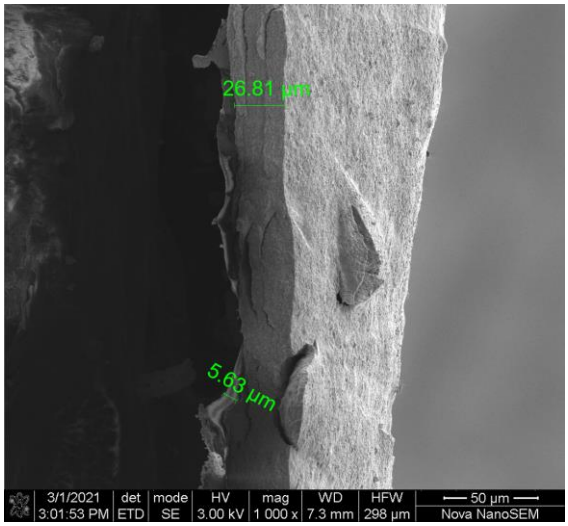

Figure D3 **Cross-section wholly hydrocarbon sPPB-H^+ ionomer based MEA after 3 h chronopotentiometry using Scanning Electron Microscopy (SEM). The MEA contains ~3.5 mg_{Ir} cm^{-2}, 20 wt% sPPB-H^+ in anode and ~1.0 mg_{Pt} cm^{-2}, 20 wt% sPPB-H^+ in cathode, and a 50 µm sPPB-H^+ membrane.**